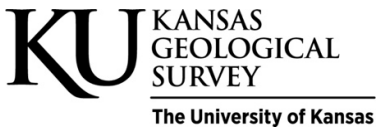
Revised High Plains Aquifer Bedrock Surface in Groundwater Management District 4 Incorporating Airborne Electromagnetic Data

by

Geoffrey C. Bohling, Brownie Wilson, Seogi Kang, Jared Abraham,

and James J. Butler, Jr.

Kansas Geological Survey Open-File Report No. 2026-38



1930 Constant Ave., Lawrence, KS 66047 • (785) 864-3965 • www.kgs.ku.edu

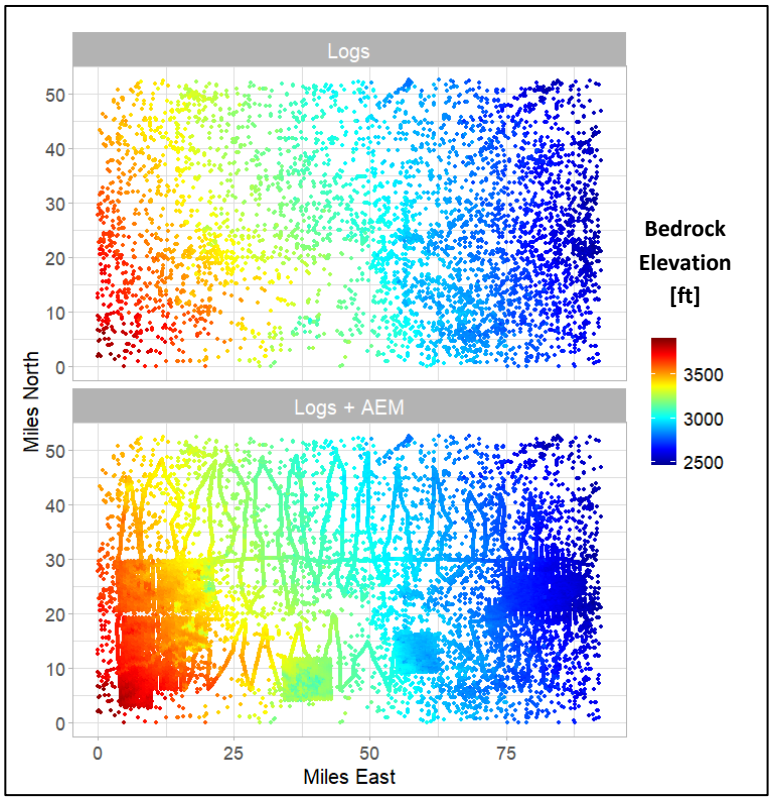
Disclaimer: The Kansas Geological Survey does not guarantee this document to be free from errors or inaccuracies and disclaims any responsibility or liability for interpretations based on data used in the production of this document or decisions based thereon.

Kansas Geological Survey

Revised High Plains Aquifer Bedrock Surface in Groundwater Management District 4 Incorporating Airborne Electromagnetic Data

Geoffrey C. Bohling [1], Brownie Wilson [1], Seogi Kang [2], Jared Abraham [3], and James J. Butler, Jr. [1]

[1]Kansas Geological Survey, [2]University of Manitoba, [3]Aqua Geo Frameworks, LLC



Kansas Geological Survey Open-File Report No. 2026-38
September 2026

GEOHYDROLOGY

KU KANSAS GEOLOGICAL SURVEY
The University of Kansas

Introduction

For more than 16 years, the Kansas Geological Survey (KGS) has developed groundwater flow models for four of the five Groundwater Management Districts (GMDs) overlying the High Plains aquifer (HPA) in Kansas. These models are updated periodically as part of the KGS Aquifer Modeling Maintenance Program. The most recent updates are for GMD4 in northwest Kansas (Wilson et al., 2021), GMD1 in west-central Kansas (Wilson et al., 2015), GMD3 in southwest Kansas (Wilson et al., 2024), and GMD2 in south-central Kansas (Wilson et al., 2020). A critical element in the development of these models is the definition of the large-scale flow system geometry. In the vertical direction, this geometry is determined by the elevations of the land surface, water table, and bedrock surface, from top to bottom. Bedrock formations are typically significantly less permeable than overlying HPA materials, and the bedrock surface is often treated as an impermeable lower boundary in groundwater flow models. The water table, which varies over time, separates the unsaturated (or vadose) zone above from the saturated zone below. The saturated zone, between the water table and bedrock, is the zone from which water can be readily pumped and thus the primary focus of both resource management decisions and groundwater flow models. The saturated zone thickness (also referred to as "aquifer thickness") represents the remaining available groundwater resource in an area. Accurate estimates of both water table elevation (or water level) and bedrock elevation are required to obtain accurate estimates of saturated zone thickness.

In the KGS modeling efforts described above, bedrock elevations have been estimated primarily from borehole sediment logs obtained by water well drillers and geologists. This report presents a revised bedrock surface for a portion of GMD4, estimated from both sediment logs and airborne electromagnetic (AEM) resistivity data obtained during a May–June 2024 survey. The survey was coordinated by Aqua Geo Frameworks, LLC (AGF), working in conjunction with the KGS, and AGF analyzed the acquired data, providing estimates of the vertical distribution of subsurface resistivity at approximately 137,000 locations (Abraham and Asch, 2024). Kang and Knight (2024) analyzed the acquired data using a different approach, designed primarily to enhance the delineation of the bedrock surface, and used the resulting resistivity estimates to generate the AEM-based bedrock picks used in this report (following correction by the KGS of a small percentage of anomalous picks).

This work was primarily supported by the Kansas Water Office through Contract 24-113. Additional support was provided by the Kansas Water Plan through the Ogallala Technical Support Program of the KGS.

Study Area

Figure 1 shows the elevation of the bedrock surface used in the existing GMD4 groundwater flow model (Wilson et al., 2021). The model grid is larger than GMD4, extending into adjacent portions of Colorado and Nebraska and regions outside the saturated extent of the HPA (treated as inactive cells in the model). The grid cells are 0.5 miles (2,640 ft) on a side, with 360 cells in the east-west (X) direction and 186 cells in the north-south (Y) direction, thus extending 180 miles in X and 93 miles in Y. The model grid coordinates are in a customized Albers projection, which is also employed in this study (although the data sets provided with this report include both latitude and longitude and UTM coordinates).

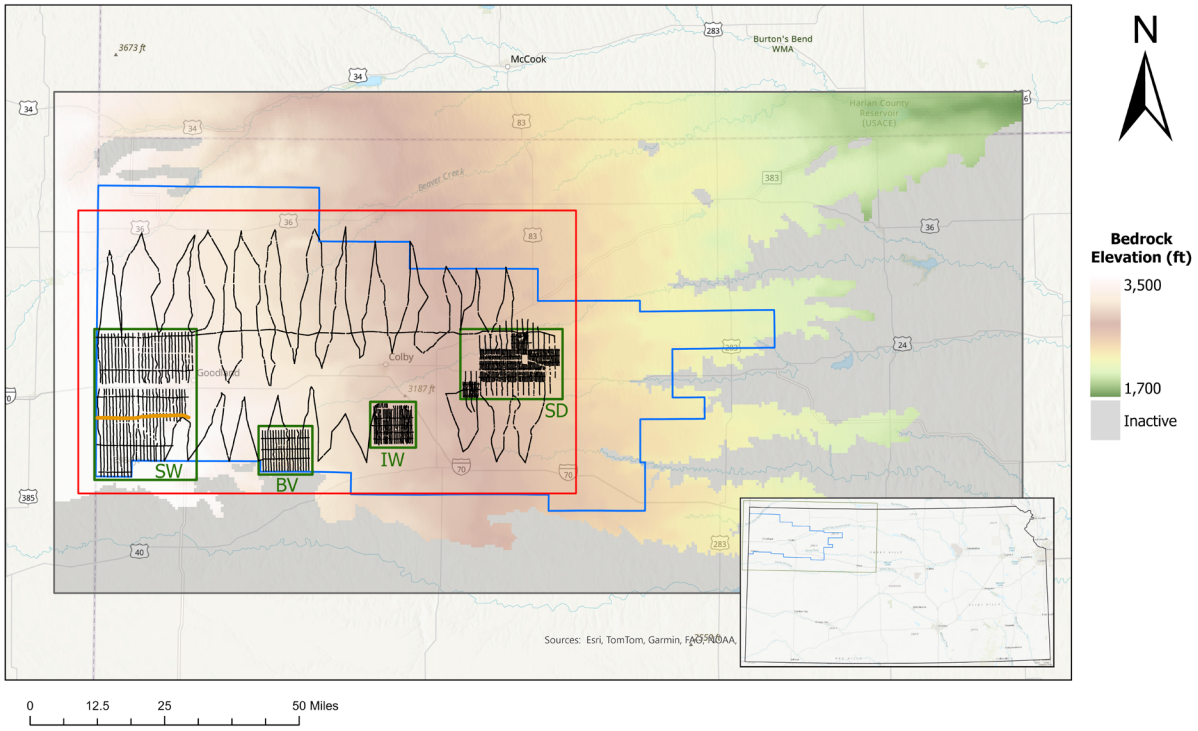


Figure 1. Original bedrock elevation over model grid (color fill, with gray areas representing inactive cells) with GMD4 boundary (blue), focus area for this report (red rectangle), and AEM flight lines (black). Green rectangles surround the four detailed survey areas: southwest (SW), Brownville (BV), Thomas County index well (IW), and Sheridan-6 LEMA (SD). Example flight line (fig. 7) is highlighted in orange. Inset map shows model grid (green) and GMD4 (blue) boundaries on a map of Kansas.

AEM survey flights covered approximately 2,500 line-miles over the central portion of GMD4, with four detailed survey regions connected by more widely spaced reconnaissance lines (fig. 1). The survey was designed to assess conditions in the "core" of the HPA in GMD4, avoiding marginally saturated regions to the east and north, with the detailed survey areas focused on regions of particular interest. Consequently, this study is focused on a rectangular region bounding the AEM survey and, to better represent the detail provided by the AEM data, develops

the revised bedrock surfaces using a finer grid within this region. This 740 x 420 grid with 1/8-mile (660-ft) grid cells covers 92.5 miles in X and 52.5 miles in Y (red rectangle in fig. 1). This fine grid is embedded within the model grid, with 16 fine-grid cells (a 4x4 block) per model grid cell.

Throughout most of the survey region, the Pierre Shale underlies the HPA, resulting in a distinctive contrast between the higher-resistivity aquifer materials (resistivities generally greater than 10 Ohm-m) and the lower-resistivity shale (resistivities generally less than 10 Ohm-m) (fig. 2). In the southeast corner of the region, the Pierre is significantly thinner and the underlying Niobrara Chalk, with resistivities similar to the aquifer, is closer to the base of the aquifer but does not appear to be directly in contact with it.

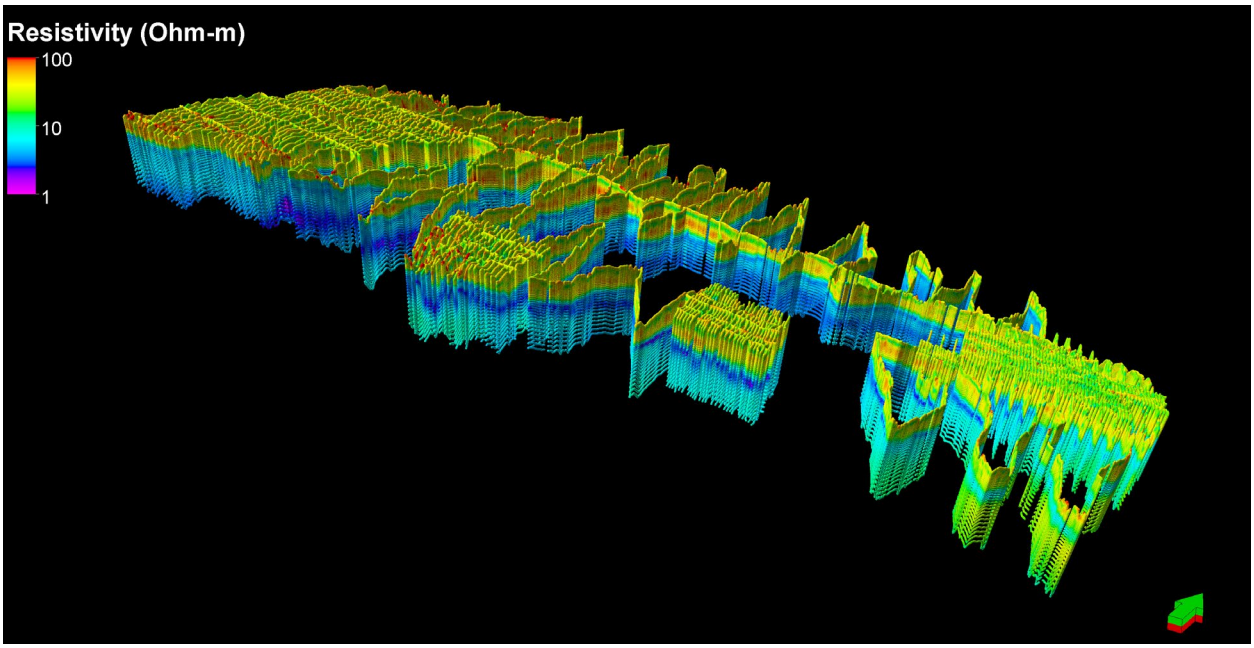


Figure 2. View of AEM resistivity data from southeast and above (north arrow in lower right corner). Data are shown from a depth of 656 ft (200 meters) upward. Data extent is 86 miles west to east and 46 miles south to north (AEM flight lines in fig. 1), and vertical exaggeration is 50x.

Bedrock Data Sources

Two bedrock surfaces are developed in this study: one based on borehole sediment logs prepared by water well drillers and geologists and another based on those logs plus AEM data. Data locations are shown in fig. 3. This section briefly discusses the nature of these data.

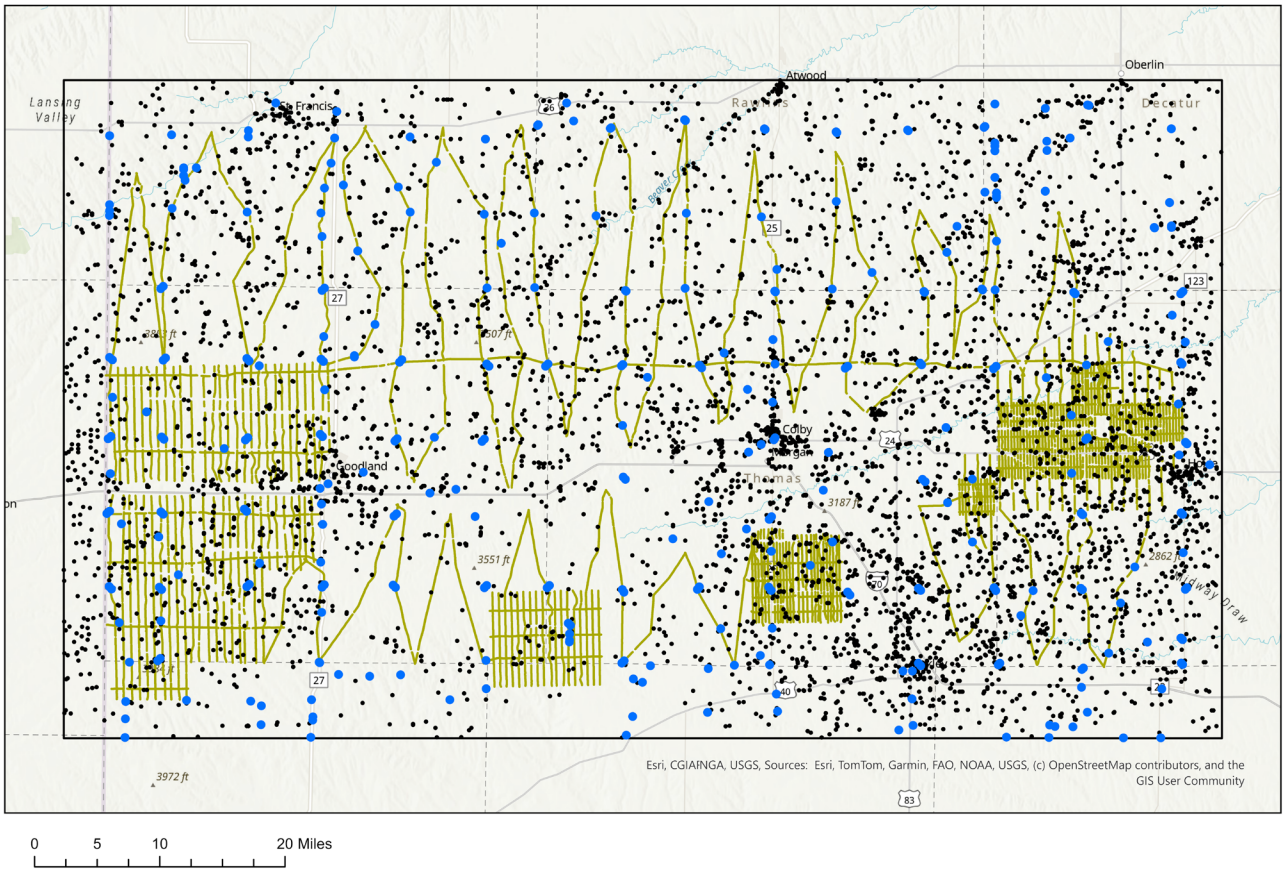


Figure 3. Locations of well logs (black), geological logs (blue), and AEM soundings (green) used to estimate the bedrock surface in the GMD4 study area (black box). More widely spaced (reconnaissance) AEM flight lines were designed to fly over as many geological logs as possible.

Sediment Logs

As mentioned above, previous bedrock elevation estimates have been developed primarily from bedrock depth picks in borehole sediment logs. Such sediment logs can be divided into two classes: those prepared by water well drillers and those prepared by geologists. This report will refer to the former as well logs (although they were obtained during drilling, prior to well installation) and the latter as geological logs. Well logs vary widely in quality but are considerably more abundant than the more carefully prepared geological logs. Nevertheless,

bedrock depth picks are probably reasonably accurate even in lower-quality well logs because drillers are familiar with the bedrock characteristics.

The majority of well logs used in this study are drawn from the KGS WWC5 database (https://www.kgs.ku.edu/Magellan/WaterWell/index.html), which contains logs associated with completed water wells in Kansas. The number of WWC5-based bedrock picks used in this study is 6,782; however, these picks are most likely not from 6,782 distinct logs, an issue discussed further below. In addition, 290 bedrock depth values listed in the Survey's water level (WIZARD) database and 149 bedrock depth values in Colorado, obtained from the USGS National Water Information System, are included in the analysis and designated as well logs in fig. 3.

The geological sediment logs employed in this study are from KGS county geological bulletins dating from the 1940s through the 1960s (Frye, 1945; Prescott, 1952, 1953; Bayne, 1956; Walters, 1956; Hodson, 1969) and a 1969 report prepared jointly by the KGS and the USGS (Keene et al., 1969).

Figure 4 shows a typical well log and a typical geological log. Throughout the region, a thin layer of yellowish weathered shale, often referred to as "ochre" in well logs, is typically observed at the top of the Pierre, providing a distinctive indication that the borehole has reached bedrock and lending increased confidence to bedrock picks from well logs. It is possible that a driller could stop too early due to encountering yellow clay within the aquifer sediment sequence, but drillers typically have reasonably accurate expectations regarding bedrock depth prior to drilling in a particular location. In addition, cross-validation interpolation has been used to identify outliers in the log-based bedrock elevations, and the provided dataset excludes these outliers.

There are two vintages of log-based bedrock picks in the provided dataset: an earlier one taken from Macfarlane and Wilson (2006) and a new one associated with this report. The earlier vintage is referred to as TS20 (for "Technical Series 20") in the dataset and the new one is referred to as OFR26-38. The TS20 picks include 2,695 WWC5 logs, 159 county bulletin logs, 290 WIZARD database records, and 149 NWIS records (in Colorado). The OFR26-38 picks include 4,087 WWC5 logs, 106 county bulletin logs, and 98 logs from Keene et al. (1969). There is almost certainly overlap between the sets of logs contributing to the two vintages of bedrock picks, for two reasons: 1) unique log IDs (e.g., WWC5 well IDs) were not retained in the TS20 dataset, and 2) most log locations are derived from "legal" location descriptions in the Public Land Survey System (PLSS) (Suchy, 2002) and are therefore subject to uncertainty. PLSS coordinates have been converted to geographic coordinates using an online tool for Kansas (https://maps.kgs.ku.edu/leoweb), which returns the latitude and longitude of the center of the smallest area designated by the PLSS coordinates. Most PLSS locations are reported to the

quarter-quarter-quarter section, an area that is 1/8 of a mile (660 feet) on a side, but some are reported only to the quarter-quarter or quarter section. Multiple logs may fall within the same PLSS designation and thus be assigned the same location.

A

Lithologic Log (Log data entered by KGS.)	
From: 0 ft. **to** 40 ft.	top soil
From: 40 ft. **to** 46 ft.	sand
From: 46 ft. **to** 85 ft.	sand, clay
From: 85 ft. **to** 91 ft.	sand and sand strips
From: 91 ft. **to** 115 ft.	sand, fine
From: 115 ft. **to** 122 ft.	sand, clay
From: 122 ft. **to** 150 ft.	sand and sand rock strips
From: 150 ft. **to** 156 ft.	sand rock, hard
From: 156 ft. **to** 160 ft.	good sand
From: 160 ft. **to** 172 ft.	sandy clay and sand strips
From: 172 ft. **to** 174 ft.	sand
From: 174 ft. **to** 177 ft.	sandy clay
From: 177 ft. **to** 178 ft.	ochre

B

6-38-31ccc. Sample log of test hole in the SW cor. sec. 31, T. 6 S., R. 38 W.; drilled August 1949. Surface altitude, 3,527.5 feet.	**Thickness, feet**	**Depth, feet**
Quaternary--Pleistocene		
Sanborn formation--Peoria silt member		
Silt, dark-brown	2	2
Silt and fine to very fine sand; contains stringers of soil caliche, 10 to 25 feet	23	25
Tertiary--Pliocene		
Ogallala formation		
Silt and clay, sandy, light-brown	8	33
Gravel, coarse, and some plastic silt and clay	8	41
Silt and fine sand, plastic, brown; contains sand and gravel at base	9	50
Gravel, coarse; contains a little silt and fine sand	3	53
Silt and fine sand, plastic, brown; contains sand and gravel	8	61
Mortar bed, soft	18	79
Sand, medium to coarse, and fine to coarse gravel	15	94
Sand, fine, and plastic silt	3	97
Sand, fine to coarse; contains some fine gravel	6	103
Sand, fine to coarse, and fine to coarse gravel	4	107
Sand, fine to coarse, and fine to coarse gravel; contains brown plastic silt and clay	6	113
Silt and clay, sandy, brown	17	130
Sand, fine to coarse, and fine gravel, partially cemented; contains some silt and very fine sand	25	155
Silt and very fine sand, plastic, brown; contains more sand from 165 to 170 feet	15	170
Silt and very fine sand, plastic, brown; contains much sand	20	190
Sand, fine to coarse; contains silt and clay	20	210
Sand, fine to medium; contains silt and clay	68	278
Cretaceous--Gulfian		
Pierre shale		
Shale, yellow-brown to greenish	1	279
Shale, dark blue-black	9	288

Figure 4. a) Typical well log, from the WWC5 database. b) Typical geological log, from a county geological bulletin.

Because of the general spatial imprecision of the log data, no attempt has been made to eliminate overlap between the TS20 and OF26-38 data included in the provided dataset. Instead, the data are treated statistically, taking the average of all bedrock elevations within a given grid cell, regardless of data vintage or source, prior to interpolating the data to create the bedrock surface.

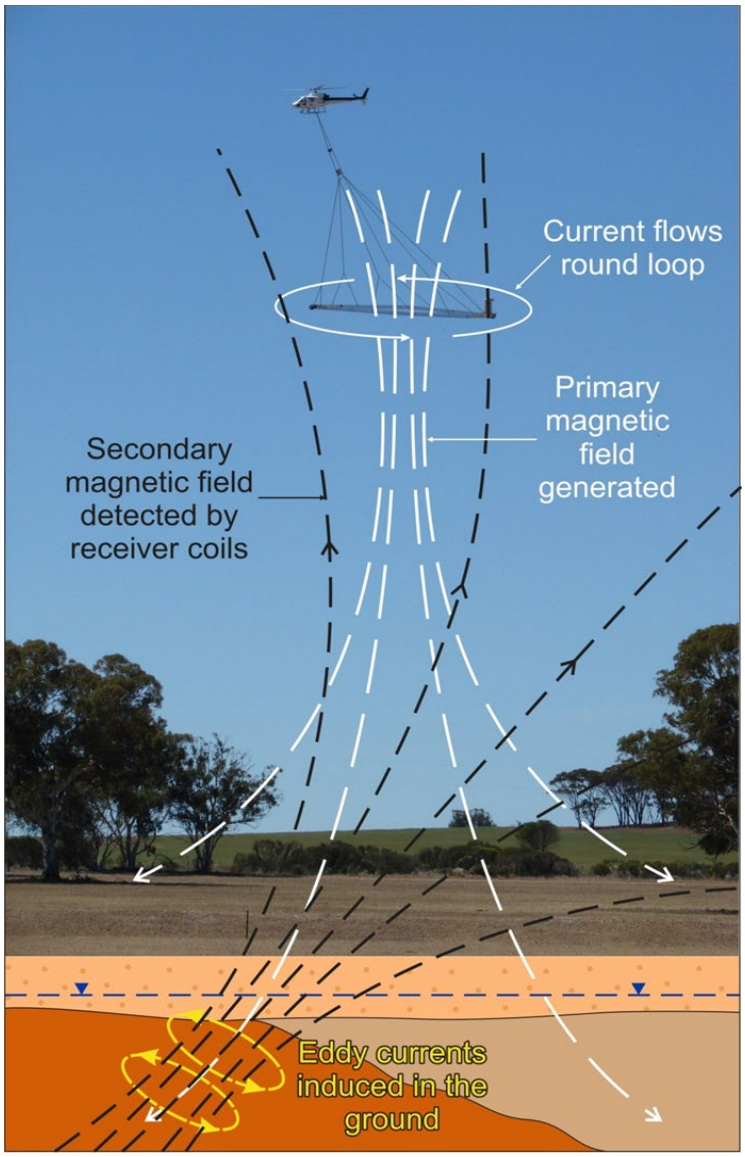


Figure 5. Schematic of how AEM works. A transmitter fires discrete electromagnetic pulses that flow around a loop and generate a primary magnetic field perpendicular to it. The magnetic field induces eddy currents in the subsurface that generate a secondary magnetic field. The AEM measurement is of this secondary field, which provides information on electrical resistivities in the subsurface. (Image courtesy of J. Abraham.)

AEM Soundings

During surveying, the AEM equipment is carried by a helicopter traveling at 50–55 mph. A transmitter generates electromagnetic pulses, creating a primary electromagnetic field that propagates into the earth. This field generates eddy currents in the subsurface that in turn generate a secondary electromagnetic field that induces a time-varying voltage response in the AEM receiver coil (fig. 5). These voltage responses are then analyzed to estimate the distribution of electrical resistivities in the subsurface. The results are represented as vertical sequences of

resistivity values at a large number of measurement locations, referred to as soundings. The flight speed combined with the time required for each measurement results in an average spacing of about 85 ft between sounding locations along flight lines, with locations recorded by GPS. However, at land surface, each sounding reflects resistivities over an area spanning approximately 100 ft perpendicular to flight lines and 200 ft along flight lines, with the longer dimension along flight lines reflecting the distance of travel during a measurement. The contributing area increases in size with increasing depth. Thus, the AEM location data are imprecise in the sense that the soundings represent areas rather than the exact (X,Y) points to which they are assigned.

The resistivity values at each sounding location are referenced to a sequence of 39 intervals that increase in thickness with depth, starting with a thickness of 2 m (6.6 ft) at land surface and increasing by a factor of approximately 1.06 with each successive interval (fig. 6). This thickness sequence, which is the same for all soundings, is a characteristic of the model used to analyze the AEM responses, with the increasing interval thicknesses designed to reflect the decreasing resolution of the data with greater depth. In this study, the bedrock depth in each sounding has been selected to minimize the variance of the logarithmic resistivity values above and below the bedrock pick (dividing the sequence into two subsequences that are as homogeneous as possible as measured by logarithmic variance). In many soundings, this corresponds to selecting the bedrock boundary based on a 10 Ohm-m threshold. In fact, the variance-based rule produced anomalous results in a small percentage of soundings, and these anomalies were corrected using a simple heuristic rule: working downward through the sounding, place the bedrock boundary at the top of the first sequence of at least six depth intervals with resistivities less than or equal to 10 Ohm-m. (At some southeast locations, where the Pierre is thin and underlain by the higher-resistivity Niobrara, the rule was modified by reducing the number of successive intervals to three.) This rule produced results that were consistent with the variance-based picks in adjacent soundings.

For both logs and AEM soundings, bedrock depths were converted to elevations by subtracting from land surface elevations extracted from a LiDAR raster (DASC, 2026). Because the AEM bedrock picks always correspond to boundaries between the resistivity depth intervals (or layers) and the same sequence of depths is used for all soundings, the bedrock depths are discretized to the interval boundary depths. This lends a jagged character to the corresponding bedrock elevations, with the bedrock surface following a certain layer boundary for some number of soundings along a flight line and then typically shifting up or down by a layer or two to continue following the bedrock resistivity contrast. To illustrate, the median AEM bedrock depth is 232.2 ft, which corresponds to the bottom of the 19th resistivity layer. The thickness of the 19th layer is 20.3 ft and the thickness of the 20th layer is 21.6 ft, so bedrock depth will decrease by 20.3 ft if it shifts upward by one layer and increase by 21.6 ft if it shifts downward by one layer from the median depth. The available depth-change increments grow in magnitude with greater depth, as

dictated by the increasing layer thicknesses. Changes in bedrock elevation reflect the discretized depth changes superimposed on the variation in land surface elevation along the flight line (fig. 7).

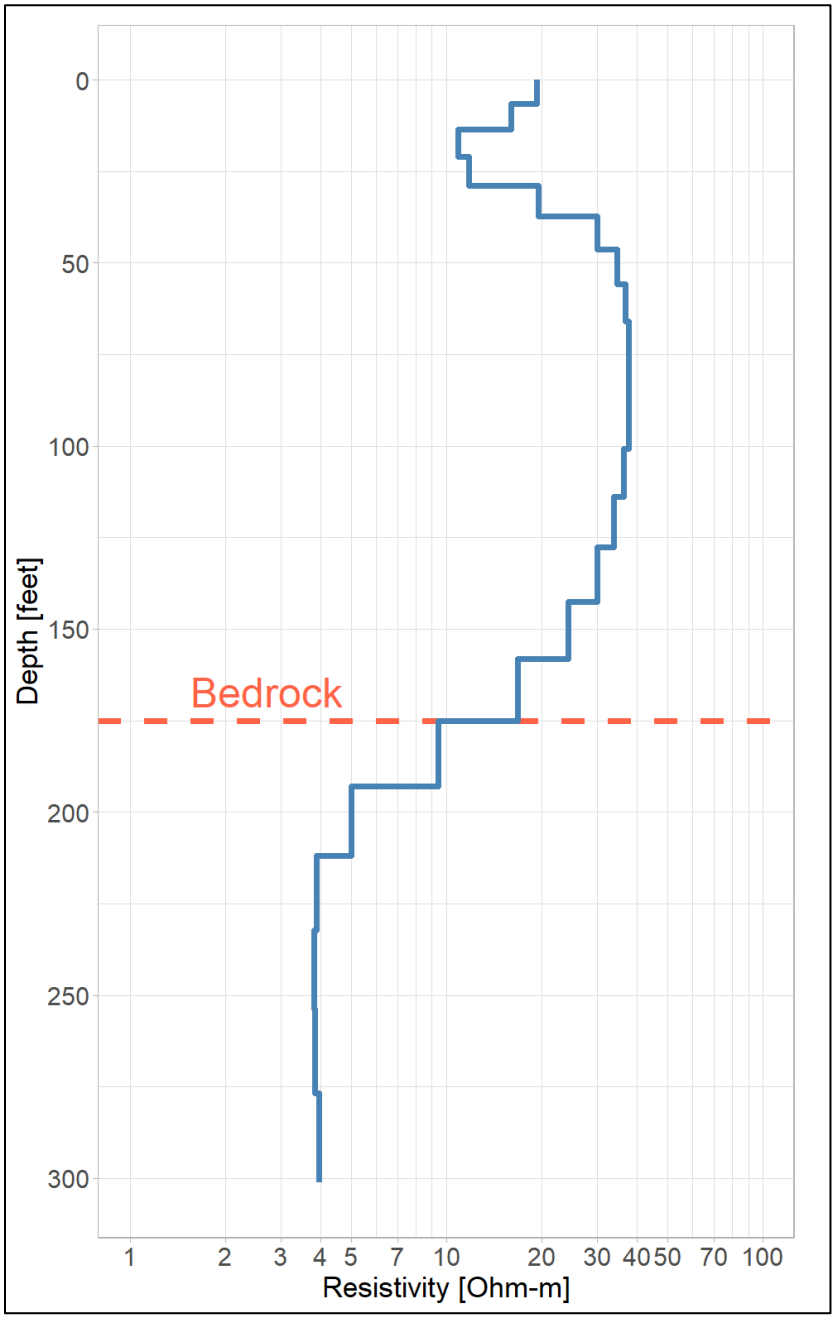


Figure 6. Estimated resistivities versus depth in a single AEM sounding with selected bedrock depth. (Sequence continues to a depth of 1,066 ft but is only shown above 300 ft.)

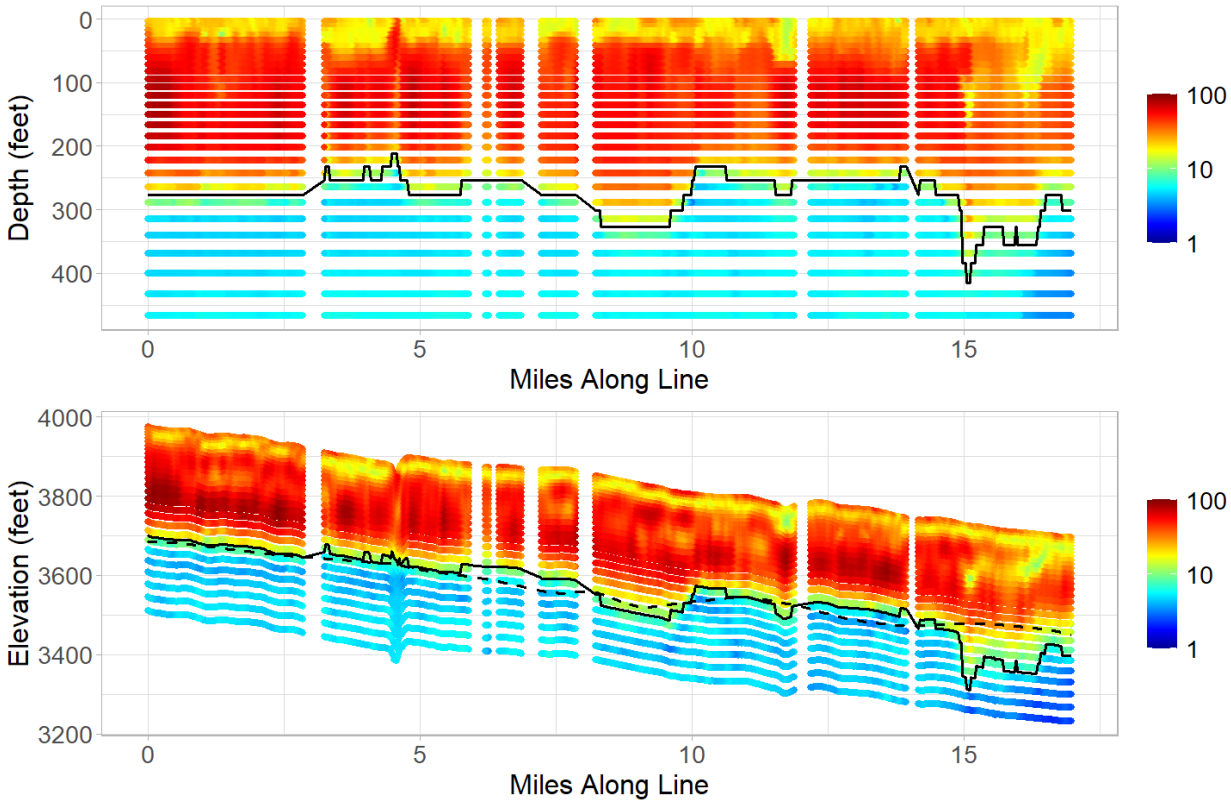


Figure 7. AEM soundings along a selected flight line (highlighted in orange on fig. 1) plotted versus depth (top) and elevation (bottom) with AEM-based bedrock picks (solid black line). Resistivity values are plotted as points at the vertical center of each depth interval (layer), and the bedrock pick in each sounding corresponds to a boundary between layers. The dashed line on the elevation plot represents bedrock elevations interpolated from log-based bedrock picks to the sounding locations.

Procedures

Aggregation to Grid Cells

Both the log- and AEM-based bedrock elevations exhibit considerable variability over short distances. In addition, multiple log-based bedrock elevations can occur at the same nominal location due to the imprecise nature of log locations and the use of two vintages of log-based bedrock picks, discussed above. To reduce the impact of this variation and create a more manageable dataset, bedrock elevations have been averaged over the 1/8-mile grid cells. This provides a natural way to integrate the two datasets simply by averaging the log- and AEM-based elevations in the same cell. In this process, the averaged elevations are assigned to the average (X,Y) location of all bedrock picks from logs and/or soundings in the cell. Figure 8 shows the grid-cell averaged elevations. Figure 9 shows the number of bedrock picks from logs and/or soundings per grid cell, and fig. 10 shows the range of elevations within each grid cell.

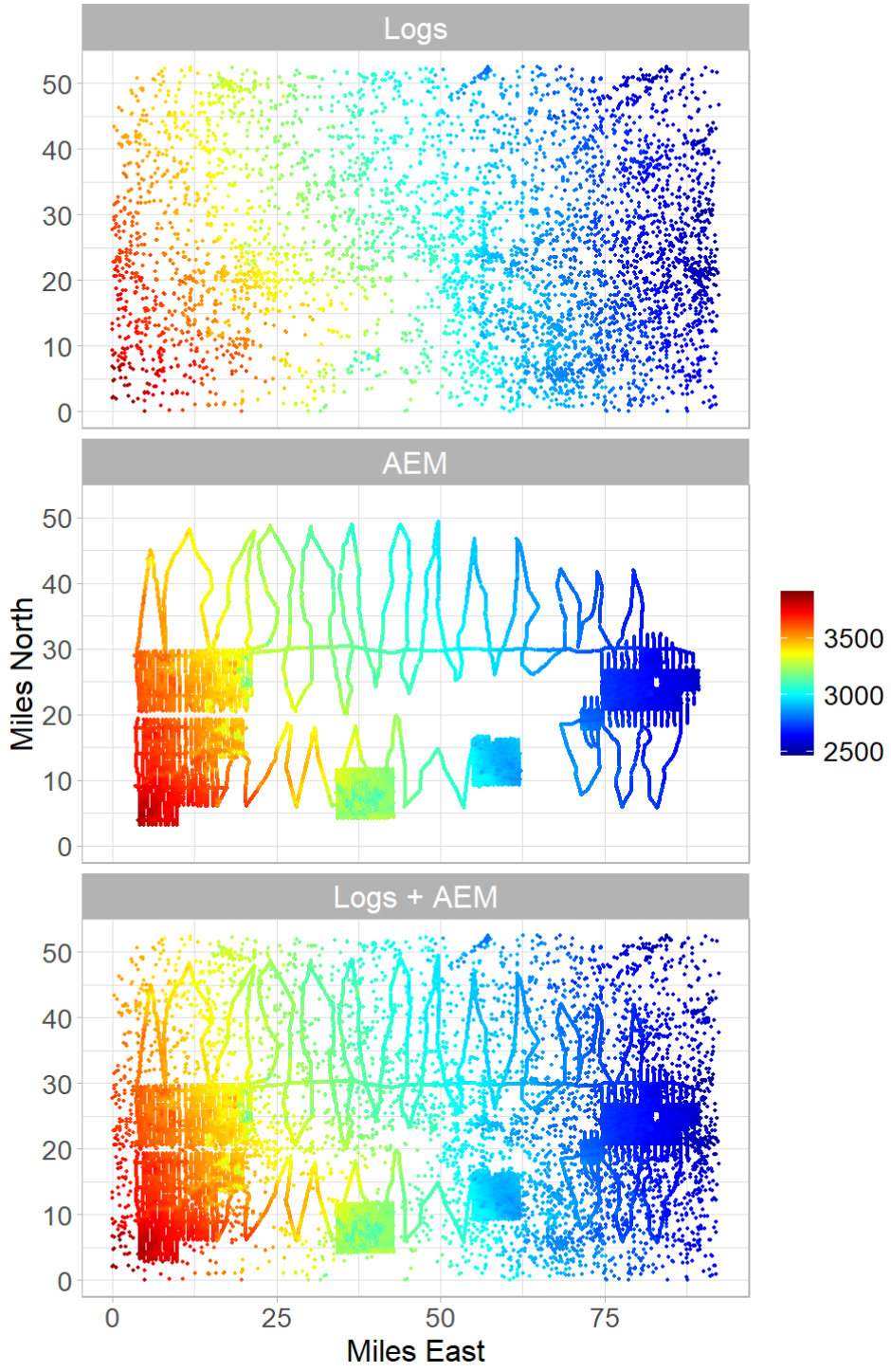


Figure 8. Bedrock elevations (ft) averaged to grid cells using logs alone (5,368 data points), AEM alone (19,547 data points), and logs and AEM together (24,595 data points). The last count is not the sum of the first two because the counts represent grid cells containing data, not original data locations.

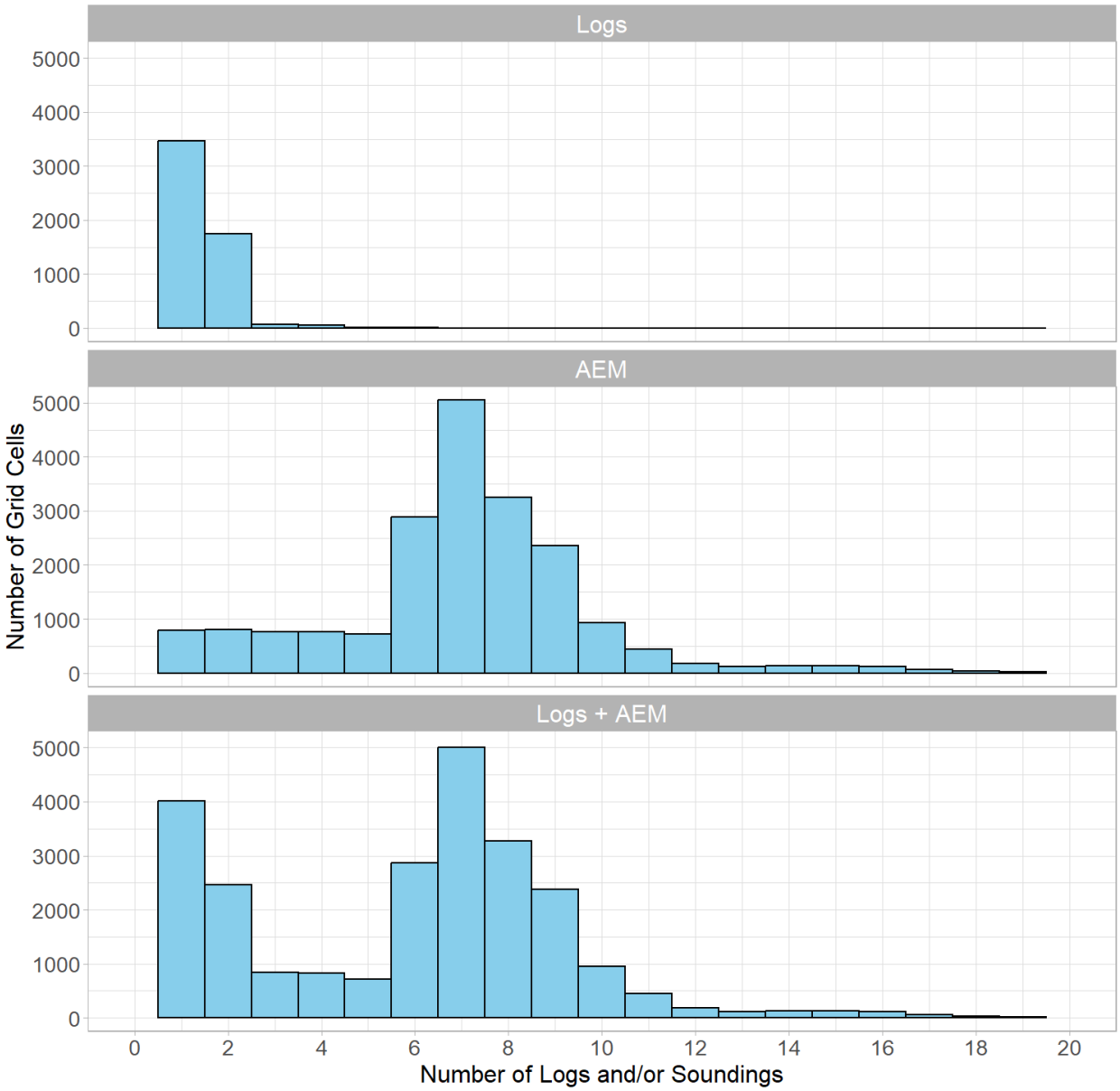


Figure 9. Distribution of the number of bedrock picks from logs and/or AEM soundings per grid cell. The number of log-based picks per grid cell ranges from 1 to 12 and the number of AEM soundings per grid cell ranges from 1 to 28 (five cells with counts greater than 20 are excluded from the plot).

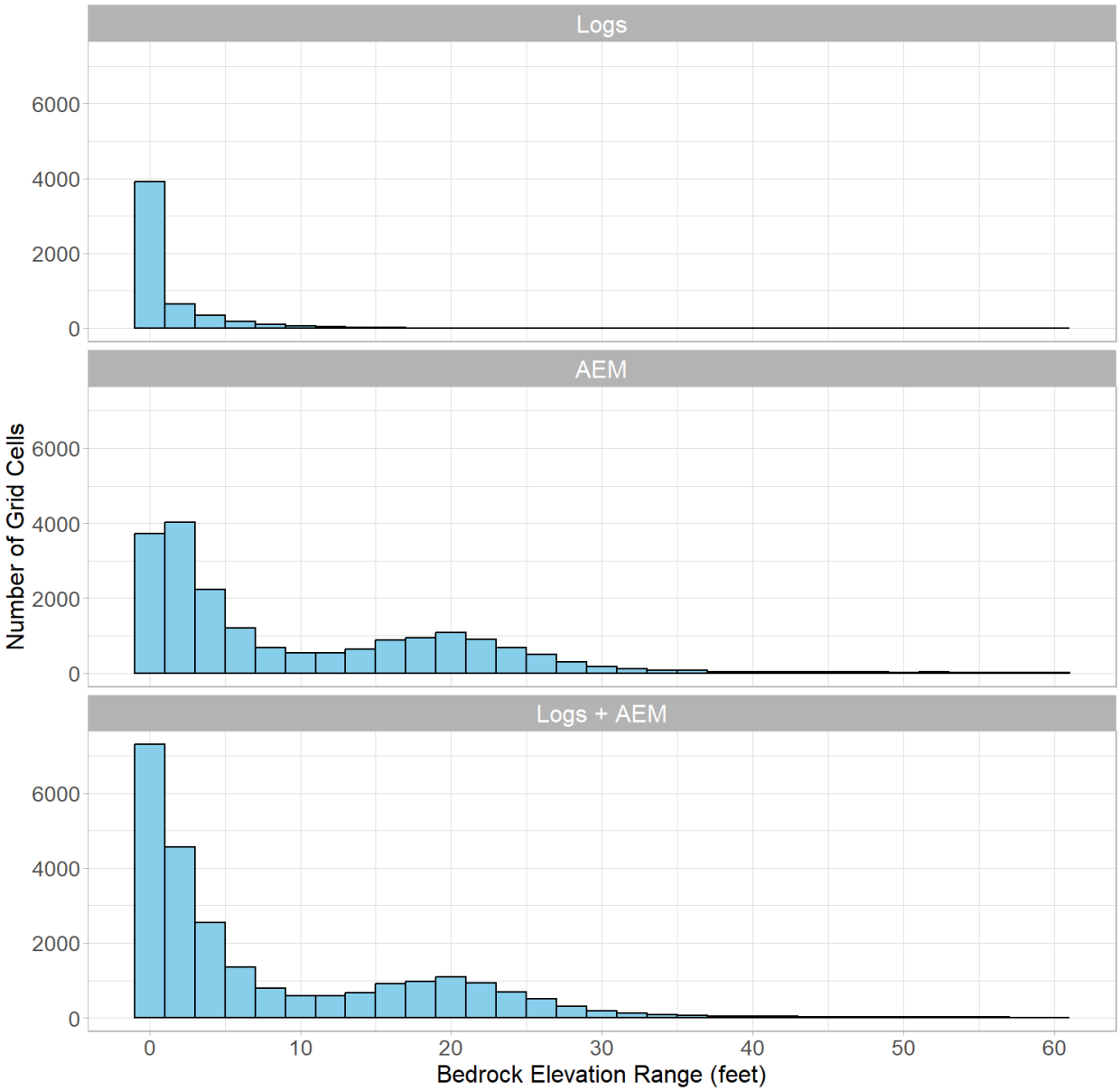


Figure 10. Distributions of bedrock elevation ranges (maximum elevation - minimum elevation) in grid cells. Elevation ranges are 0–73 ft for logs and 0–112 ft for AEM soundings. Cells with ranges greater than 60 ft (3 cells for logs alone, 50 cells for AEM alone, and 71 for the combined dataset) have been excluded from the plot.

Interpolation

The next step is to create two alternative bedrock surfaces by interpolating two of the grid-cell averaged bedrock elevation datasets—one using logs alone and one using logs and AEM together—to all grid cells. Details of the interpolation process are given in Appendix B. The AEM-only dataset is not interpolated because its very nonuniform coverage of the study area would produce a surface dominated by interpolation artifacts. Before comparing the gridded results, it is instructive to look at a more detailed comparison obtained by interpolating the grid-cell averaged log-based elevations to the individual AEM sounding locations (fig. 11, with an example comparison along the example flight line shown in fig. 7). The differences between the two range from -205 ft to 142 ft, with positive values indicating that the AEM bedrock is above the log bedrock and vice versa. Larger magnitude differences are concentrated in a few areas, most notably the Brownville focus area, where the differences also exhibit significant spatial variation. In general, the AEM-based bedrock elevations exhibit more spatial variability than is indicated by the logs, and this is particularly true in the Brownville area (discussed further later in this report). Figure 12 represents the distribution of the differences and table 1 contains summary statistics of this distribution. On average, the AEM bedrock elevations are 5.3 feet above the bedrock elevations interpolated from the logs.

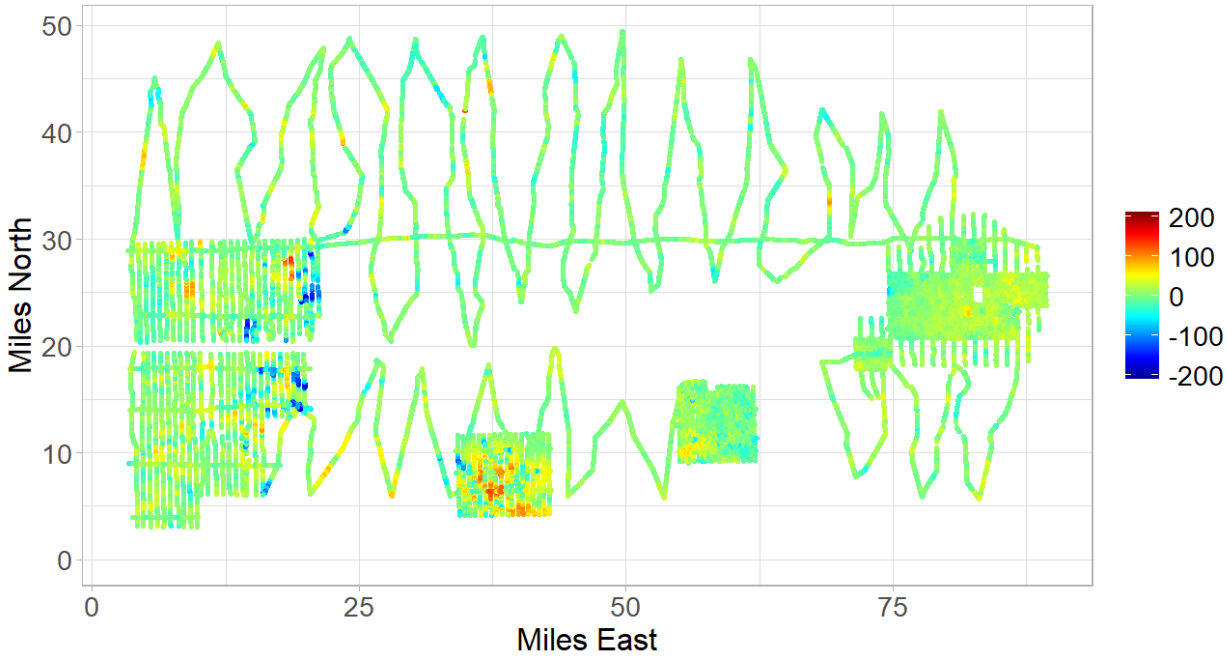


Figure 11. Difference between AEM-based bedrock elevation at each sounding location and grid-cell averaged log-based bedrock elevations interpolated to that location (ft). Positive values mean that AEM bedrock is above log bedrock and vice versa. Differences range from -205 to 142 ft.

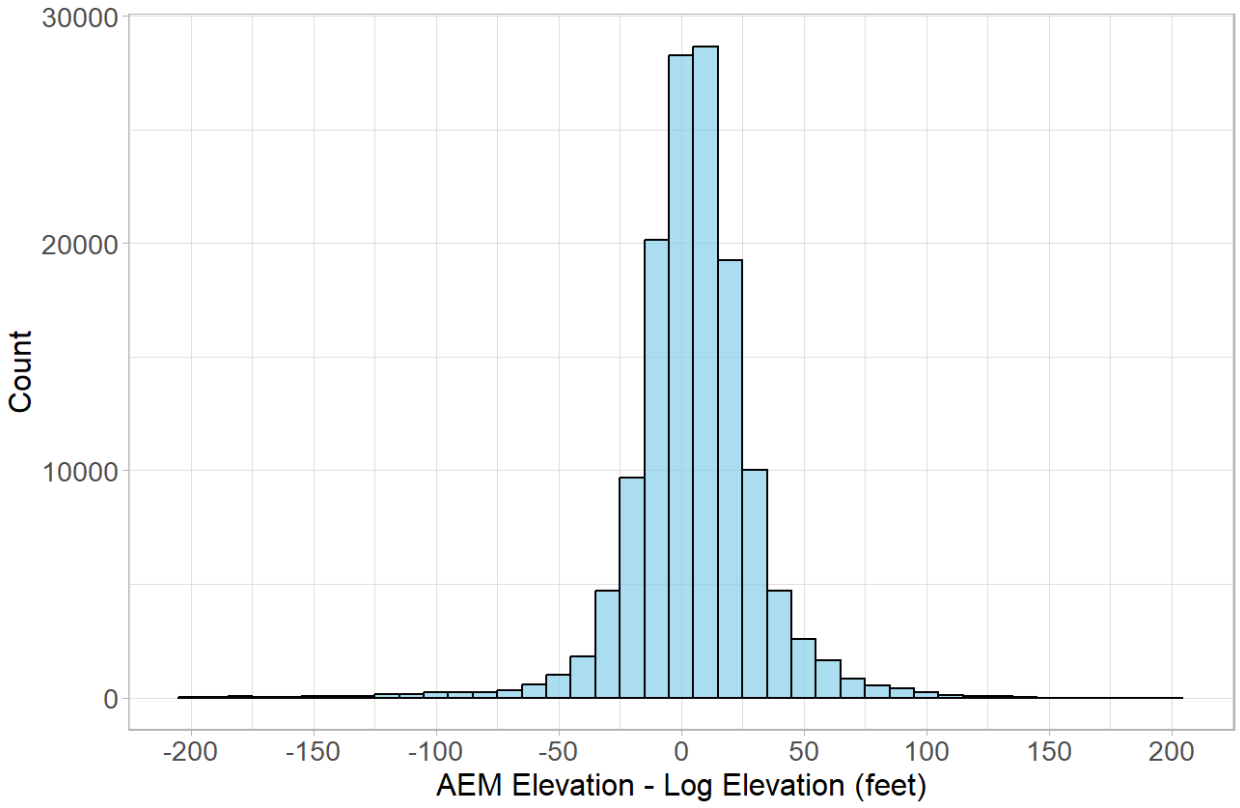


Figure 12. Histogram of differences shown in fig. 11.

Table 1. Summary statistics (ft) of differences between AEM bedrock elevations at individual sounding locations and bedrock elevations interpolated from grid cell-averaged log bedrock picks. Positive values indicate that AEM bedrock is above log-based bedrock and vice versa. SD is standard deviation and percentage values represent percentiles of the data.

Mean	SD	Min	5%	25%	50%	75%	95%	Max
5.3	25.3	-204.8	-30.0	-7.2	5.2	17.6	43.9	142.2

Figure 13 shows the bedrock surfaces estimated over the grid by interpolating from the logs-only and combined (logs and AEM) datasets. Interpolation artifacts (bull's-eyes) are apparent in both surfaces. Due to the imprecise nature of log data, one might consider smoothing the log-based interpolated surface to reduce such artifacts. However, we chose not to smooth the combined-data surface to preserve the detail provided by the AEM data and, for consistency, have also left the logs-only surface unsmoothed. The two surfaces are largely similar, although inclusion of the AEM data provides more detail in the vicinity of the flightlines.

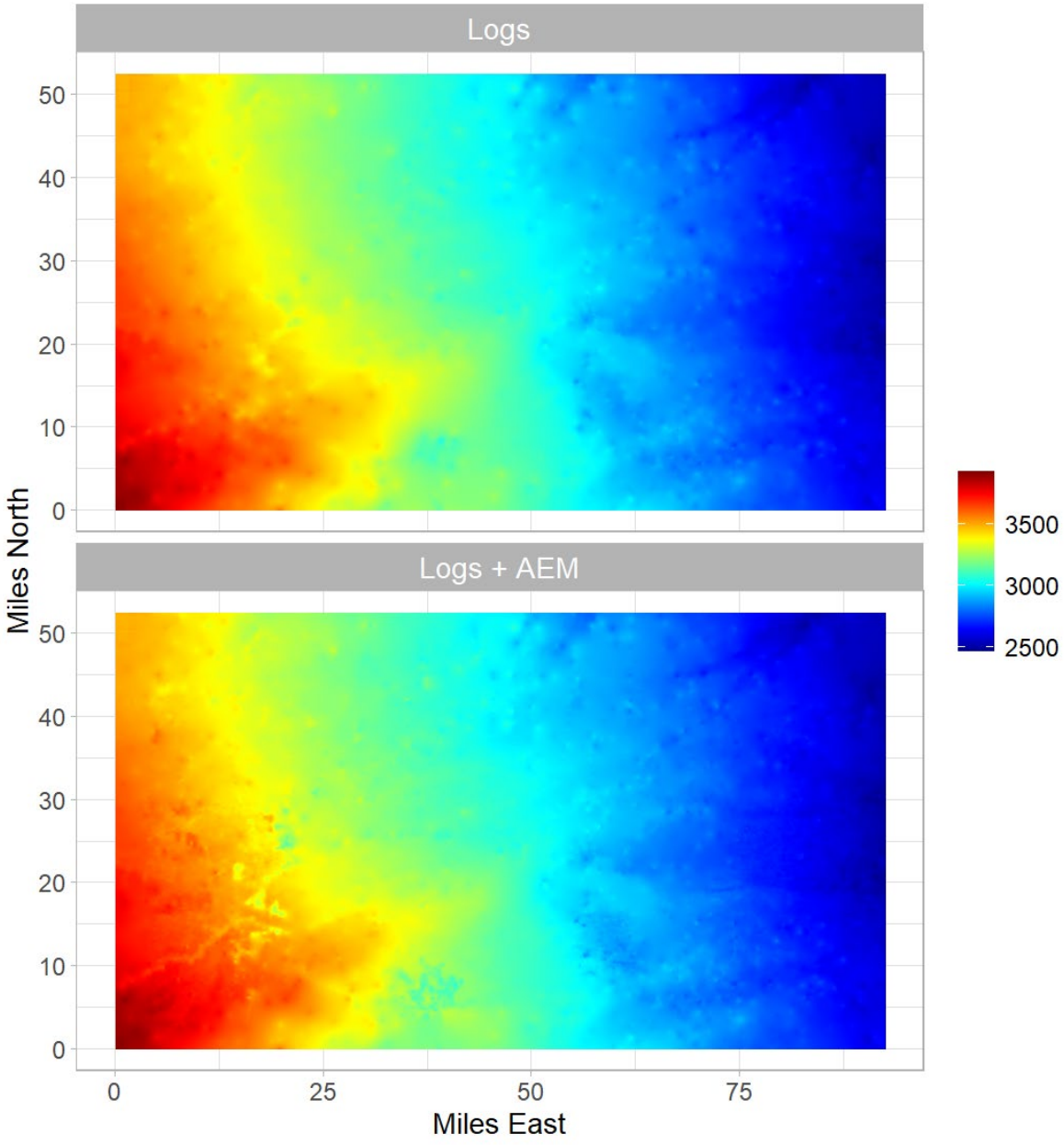


Figure 13. Interpolated bedrock elevations (ft) based on logs alone and logs and AEM combined. In both, the interpolation is from the grid-cell averaged elevations (for cells containing data) to all grid cells.

Figure 14 shows the difference between the bedrock surfaces estimated from the combined and logs-only datasets, and fig. 15 represents the distribution of those differences, with summary statistics given in table 2. Because more distant data points have less influence on the interpolation estimate at a given point, the logs dominate the interpolation estimates from the combined dataset in the gaps between the AEM flight lines; thus, the differences between the two surfaces tend toward 0 in these gaps and the distribution of differences strongly peaks at 0. Consequently, the average difference between the combined-data and logs-only surfaces (1.5 ft) is notably less than the average difference between the AEM bedrock elevations and interpolated log-based elevations at the AEM sounding locations (5.3 ft).

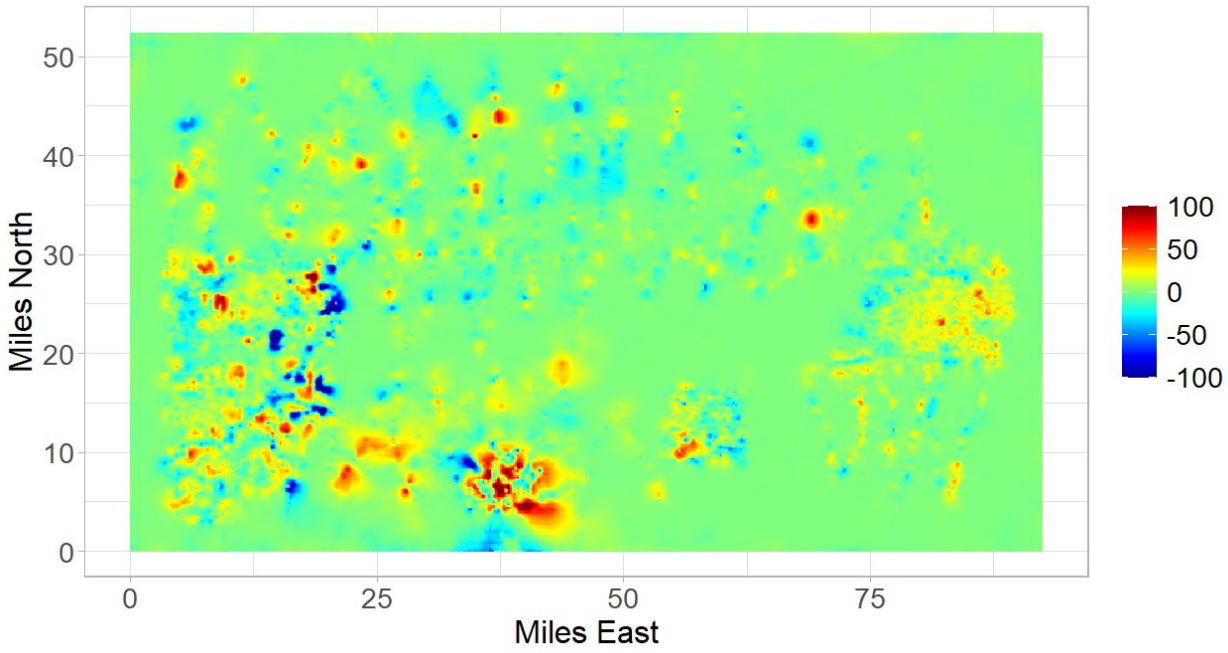


Figure 14. Difference (ft) between bedrock elevations computed from combined data (logs and AEM) and logs alone. Positive values indicate that the bedrock elevation interpolated from the combined data is above that interpolated from logs alone and vice versa. Actual differences range from -189 to 134 ft; differences greater than 100 ft in magnitude (in 367 cells, 0.1% of total) are represented as -100 or 100 ft.

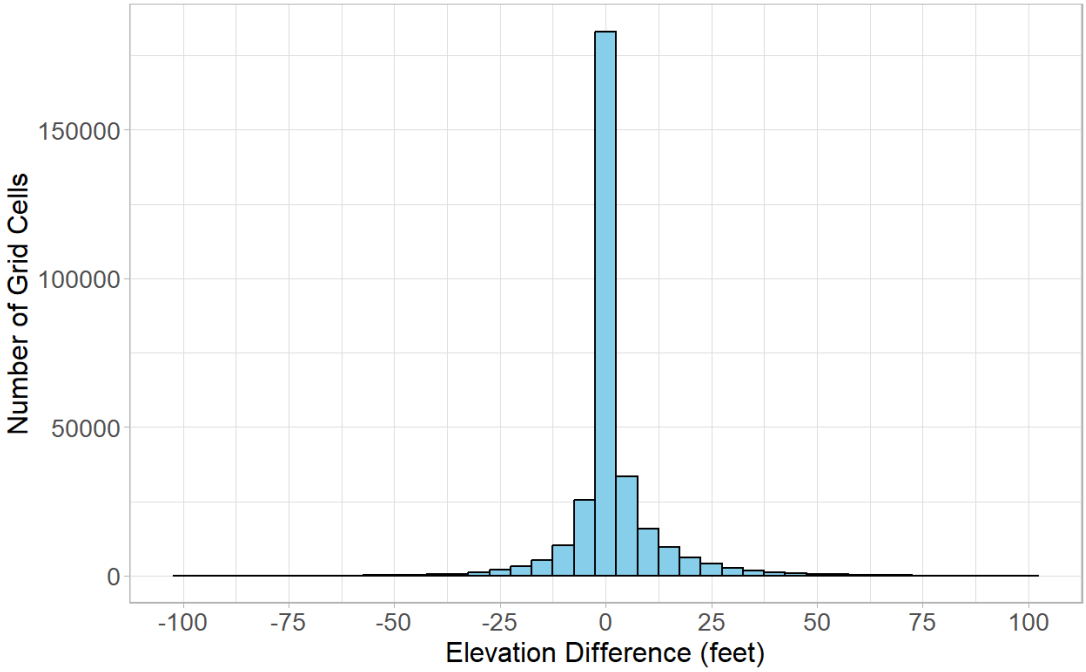


Figure 15. Histogram of differences shown in fig. 14. Bin width is 5 ft. Grid cells with differences greater than 100 ft are excluded from the plot.

Table 2. Summary statistics (ft) of differences between bedrock elevations interpolated to fine grid from combined (logs and AEM) and logs-only datasets. Positive values indicate that combined-data bedrock is above logs-only bedrock and vice versa.

Mean	SD	Min	5%	25%	50%	75%	95%	Max
1.5	12.0	-188.7	-11.7	-0.8	0.1	2.5	20.2	133.6

Figures 16–19 compare the logs-only and combined data interpolated bedrock surfaces in the four AEM survey focus areas in GMD4, from west to east. In all four cases, the addition of the AEM data lends considerably more detail to the results. For the southwest and Sheridan-6 focus areas, structures resembling paleovalleys are more clearly delineated in the combined-data bedrock surface. In both the Brownville and Thomas County index well areas, the logs-only results indicate a somewhat nebulously defined basin structure while the combined data results indicate a pitted terrain superimposed on that structure, especially in the Brownville area. The pitted structure on the bedrock surface could be due to dissolution of underlying evaporite formations (Macfarlane and Wilson, 2006).

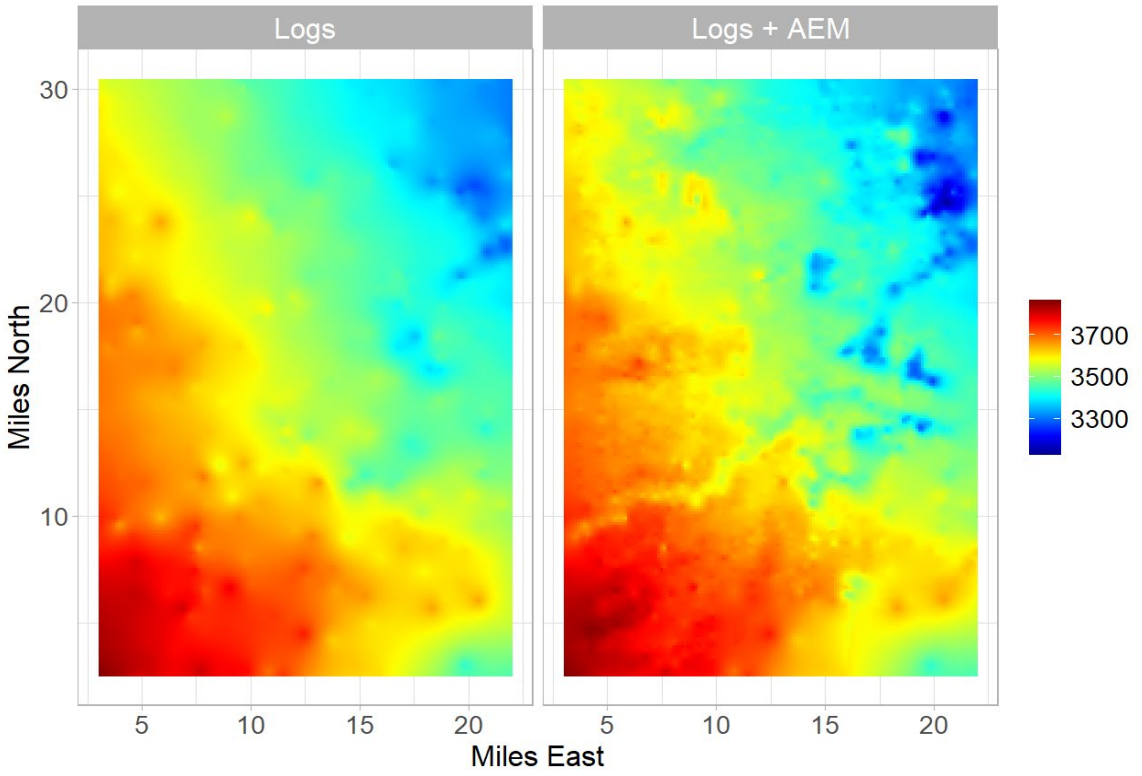


Figure 16. Bedrock elevations (ft) in southwest focus area interpolated from logs-only and combined datasets.

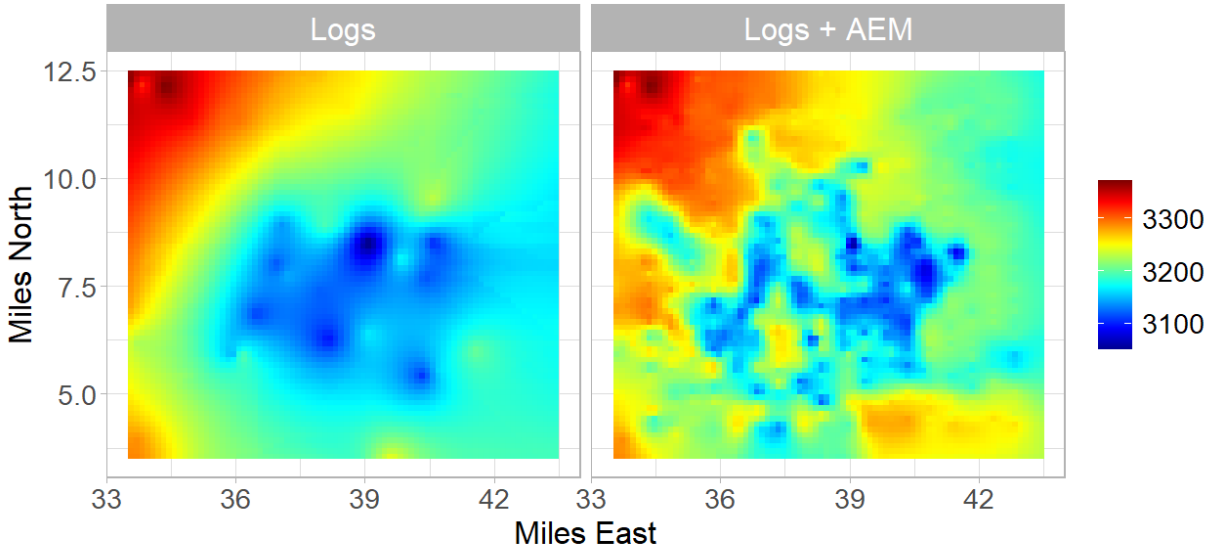


Figure 17. Bedrock elevations (ft) in Brownville focus area interpolated from logs-only and combined datasets.

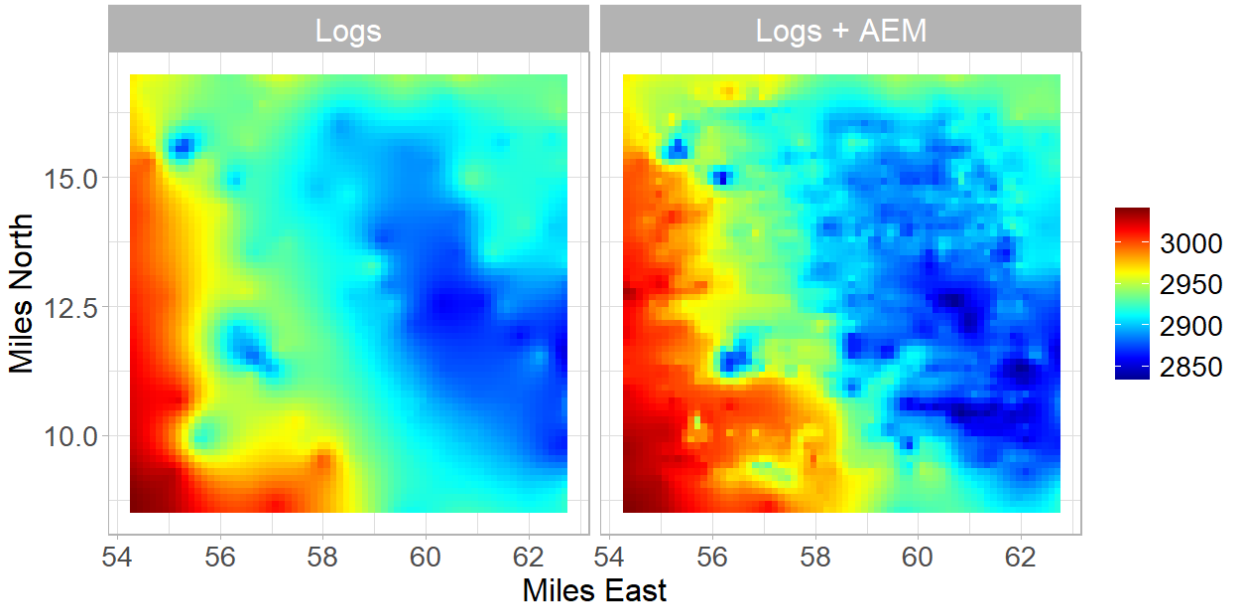


Figure 18. Bedrock elevations (ft) in Thomas County index well focus area interpolated from logs-only and combined datasets.

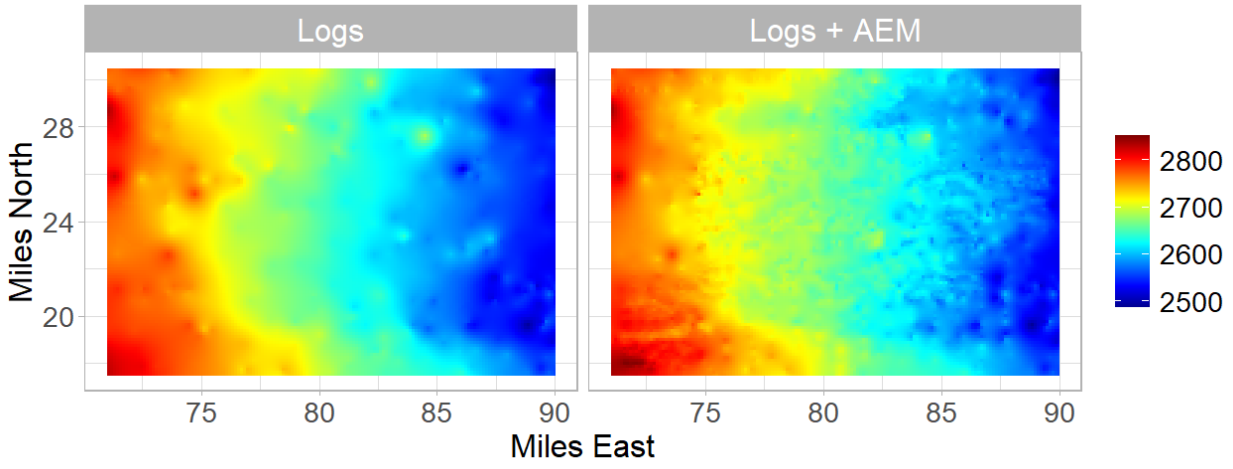


Figure 19. Bedrock elevations (ft) in Sheridan-6 focus area interpolated from logs-only and combined datasets.

Saturated Thickness and Water Use

For the sake of groundwater resource investigations, the most important impact of the new bedrock information provided by the AEM data is on the assessment of the remaining saturated thickness of the aquifer, given by the difference between the current water level and the bedrock elevation at any given location. This thickness essentially represents the remaining groundwater resource in an area, although not all the remaining groundwater can be extracted because large-volume pumping becomes infeasible once the saturated thickness falls below a certain threshold.

Aquifer productivity at a given location is determined primarily by the product of the saturated thickness and the aquifer permeability (vertically averaged over the saturated zone) at that location. Thus, one would expect to see more groundwater production in areas of greater saturated thickness. Because irrigators and other groundwater users have been searching for productive areas in the HPA for decades, the present distribution of water use should provide significant information regarding the distribution of aquifer productivity and thus saturated thickness. Consequently, a comparison between water use and saturated thickness computed using the bedrock surface estimated from the logs-only and combined datasets should provide some evidence regarding the utility of the information provided by the AEM data.

We computed saturated thickness by subtracting the two bedrock surfaces from a water level surface estimated from the averages of water level measurements obtained each January from 2020 to 2025 in 267 wells in the study area (fig. 20). This is a portion of the network of approximately 1,400 wells throughout the Kansas HPA measured annually by the KGS and the Division of Water Resources of the Kansas Department of Agriculture (Miller et al., 1999). We are comparing these saturated thicknesses to the total annual irrigation water use in each grid cell averaged over the five-year period 2020–2024 (fig. 21), which was extracted from the WIMAS database (https://geohydro.kgs.ku.edu/geohydro/wimas). (Irrigation accounts for 97.6% of the total groundwater use in the area over this period.) The reason for comparing average use over five years to the average saturated thickness computed from six annual water level measurement campaigns is that the first and last measurement campaigns (January 2020 and 2025) bracket the five-year use period.

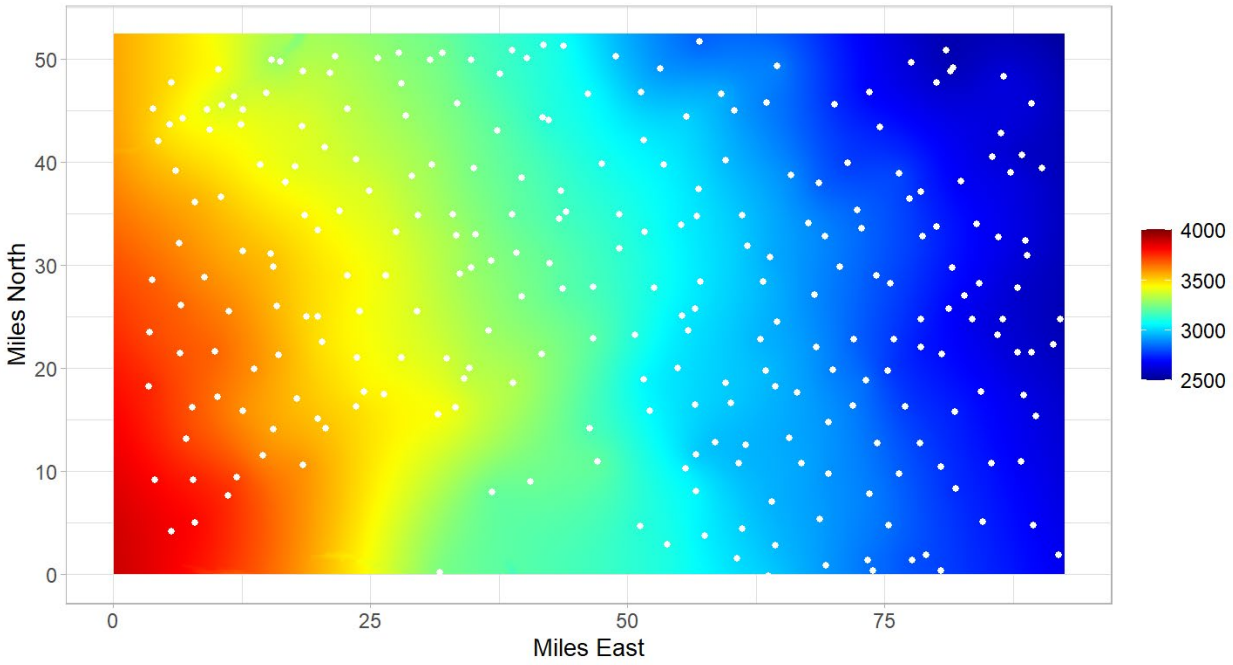


Figure 20. Water table elevation (ft) interpolated to the study area grid from averages of six annual (January 2020–January 2025) water level measurements at 267 wells (white points) in the study area.

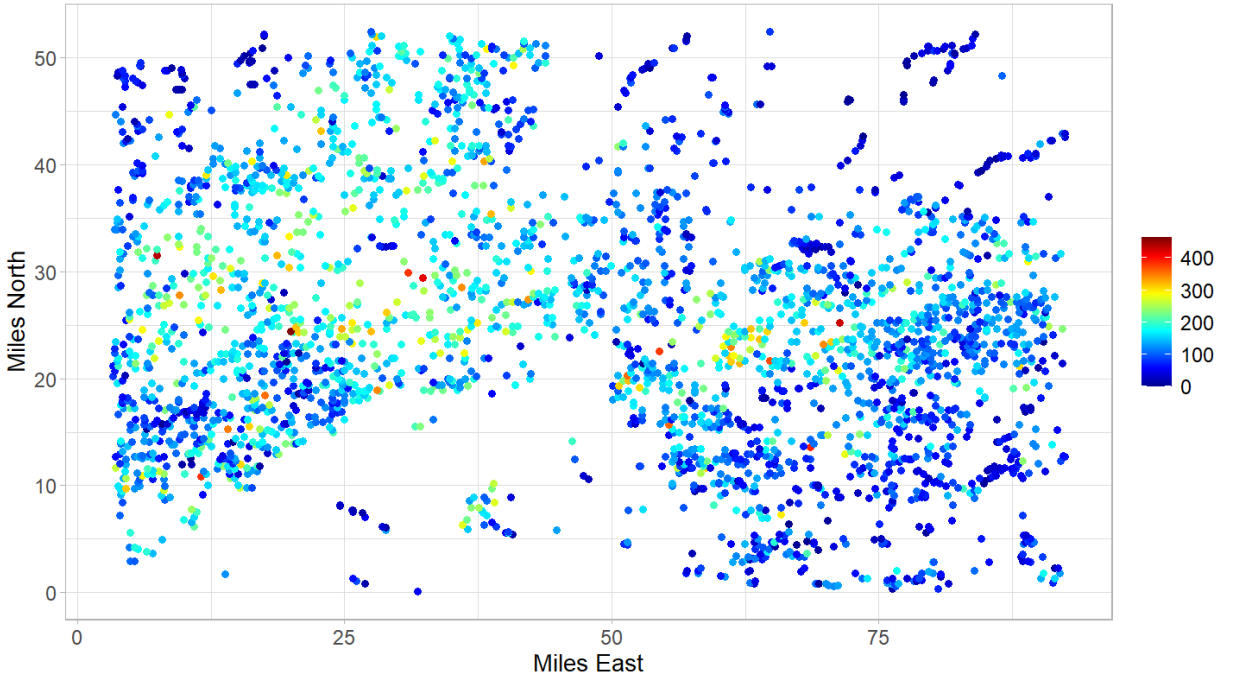


Figure 21. Average of 2020–2024 annual irrigation groundwater use (acre-ft) summed over all irrigation wells in each grid cell. Most cells contained only one active irrigation well during this period, but the number of wells per cell ranges up to six.

Figure 22 compares water use to the saturated thicknesses computed from the two bedrock surfaces. Although water use is clearly higher in areas of greater saturated thickness, it is difficult to discern differences between the two cases at this scale. More detail is revealed in plots of the four focus areas (figs. 23–26). In the southwest and Sheridan-6 focus areas (figs. 23 and 26), some concentration of higher water use values is evident along regions of higher saturated thickness. The higher values correspond to the channel-like structures seen in figs. 16 and 19 that are more clearly defined by the combined dataset. The Brownville and Thomas County index well focus areas (figs. 24 and 25) show a clear correspondence between higher water use values and the pockets of larger saturated thickness corresponding to bedrock depressions, which are again more clearly delineated by the combined dataset; the correspondence is particularly striking in the Brownville focus area. These results are compelling evidence that the AEM data provide enhanced characterization of the remaining saturated thickness in these areas.

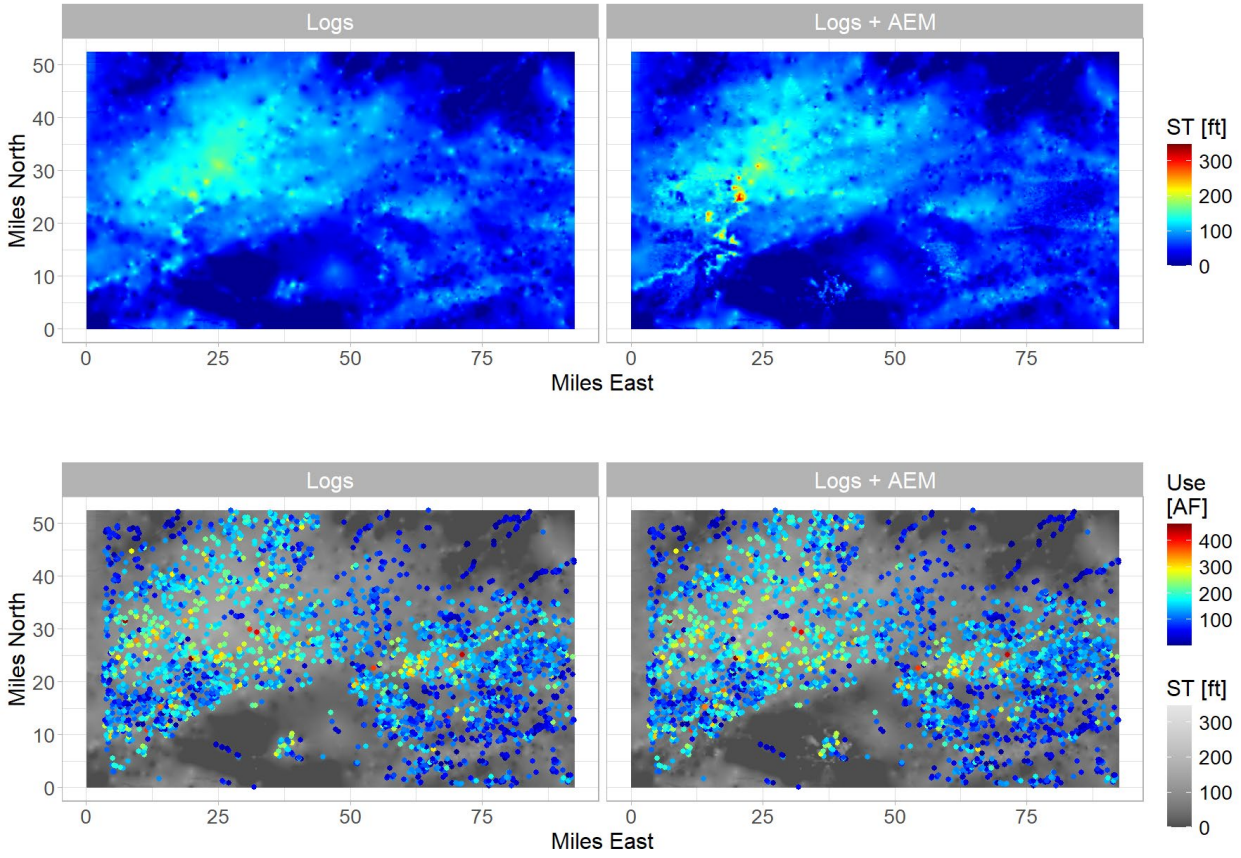


Figure 22. Average January 2020–2025 saturated thickness (ST, ft) computed from logs-only and combined dataset bedrock surfaces (top) and with 2020–2024 average irrigation water use (Use, acre-ft) superimposed (bottom) for full grid. Saturated thickness has been set to 0 in grid cells where the interpolated water table is at or below the bedrock surface (8% of cells for the logs-only dataset and 9% for the combined dataset).

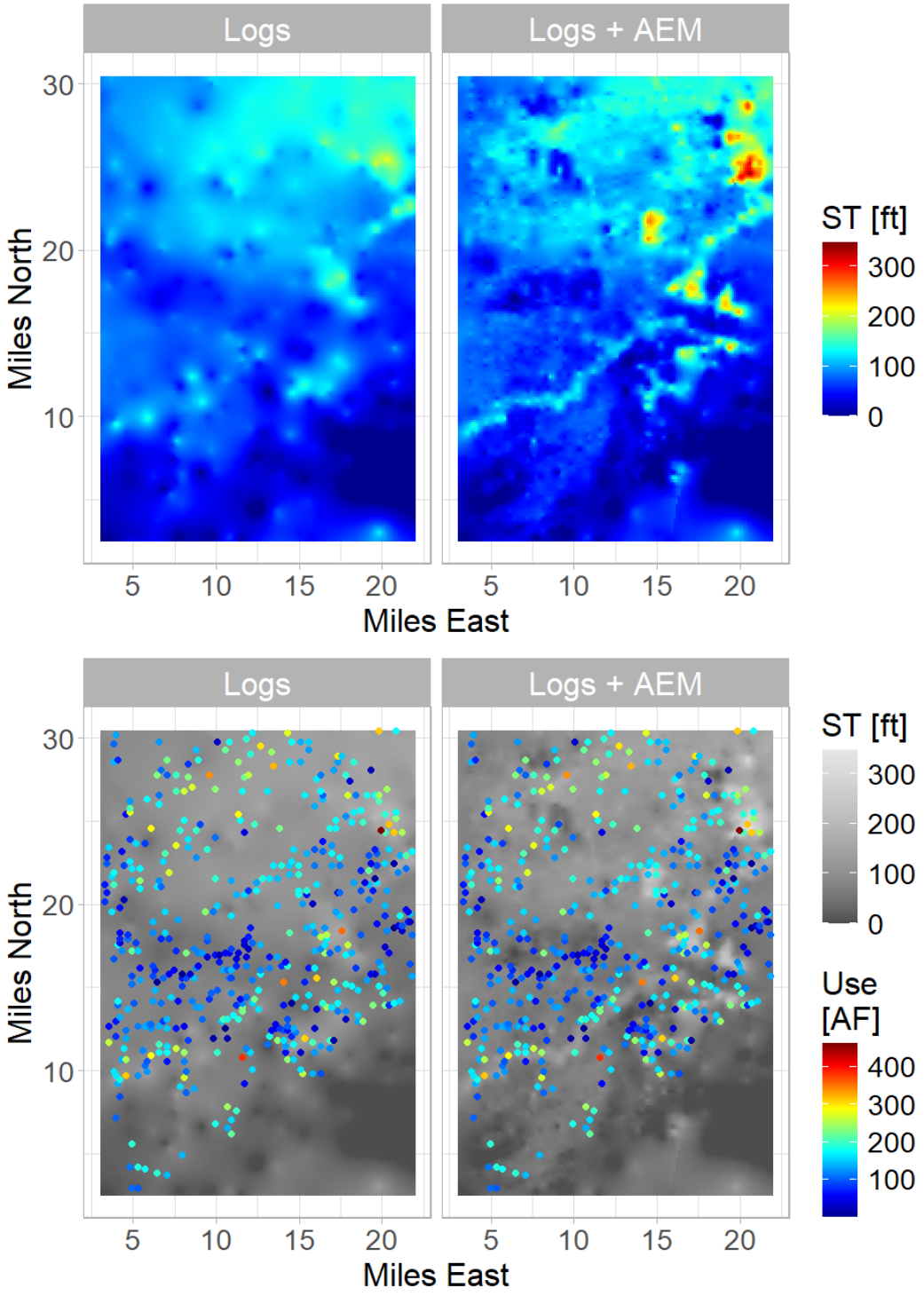


Figure 23. Average January 2020–2025 saturated thickness (ST, ft) computed from logs-only and combined dataset bedrock surfaces (top) and with 2020–2024 average irrigation water use (Use, acre-ft) superimposed (bottom) for southwest focus area.

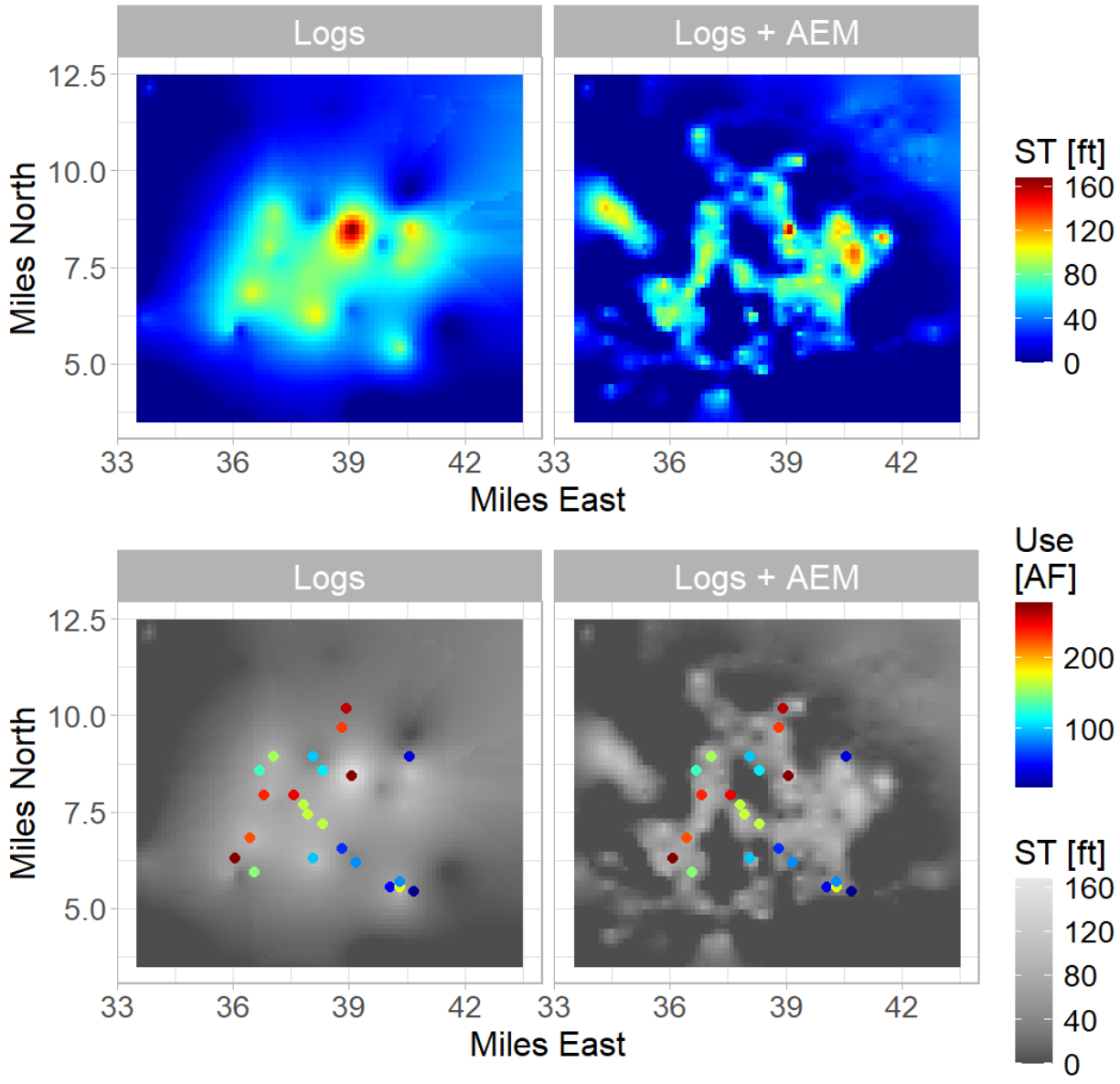


Figure 24. Average January 2020–2025 saturated thickness (ST, ft) computed from logs-only and combined dataset bedrock surfaces (top) and with 2020–2024 average irrigation water use (Use, acre-ft) superimposed (bottom) for Brownville focus area.

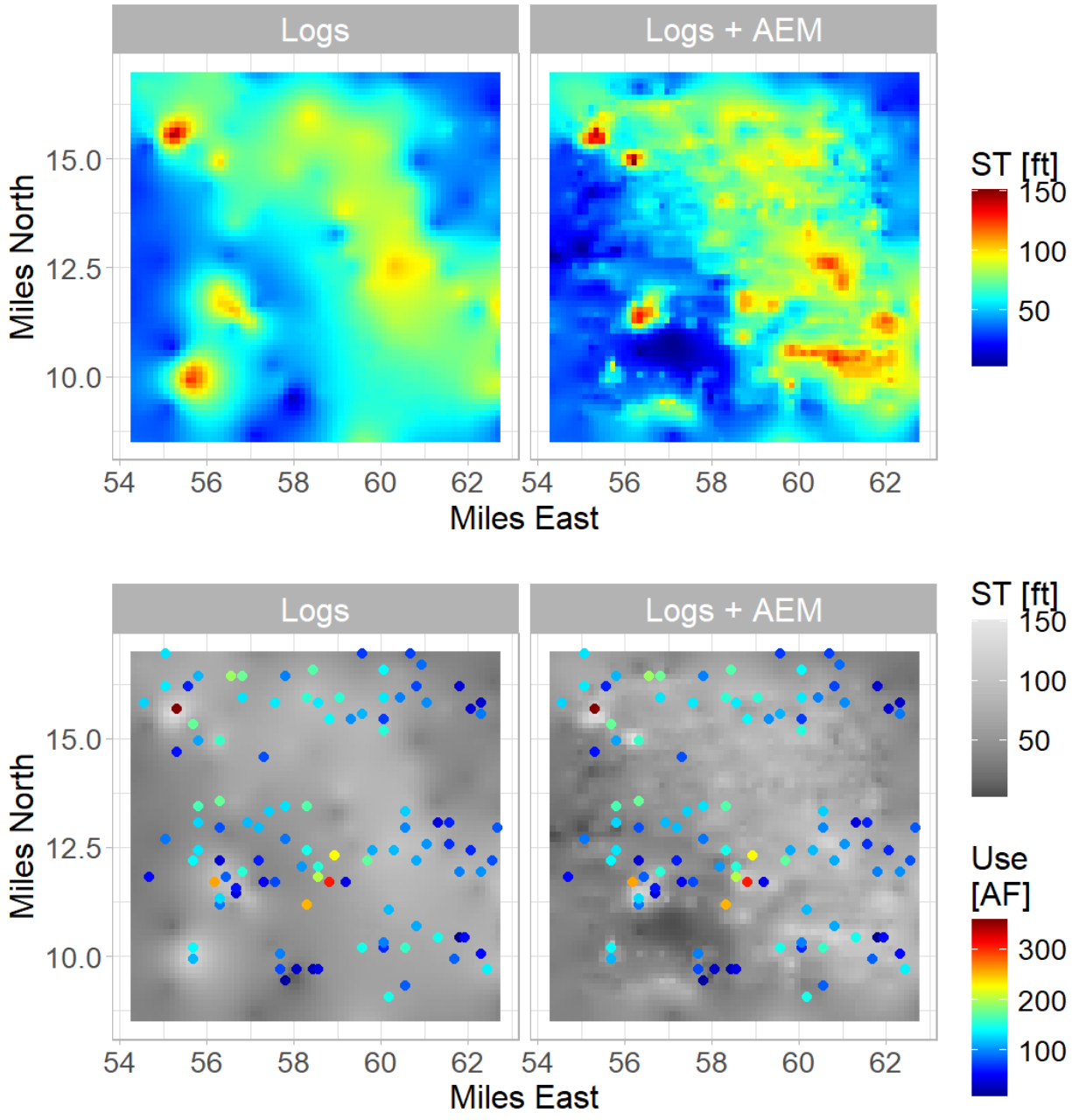


Figure 25. Average January 2020–2025 saturated thickness (ST, ft) computed from logs-only and combined dataset bedrock surfaces (top) and with 2020–2024 average irrigation water use (Use, acre-ft) superimposed (bottom) for Thomas County index well focus area.

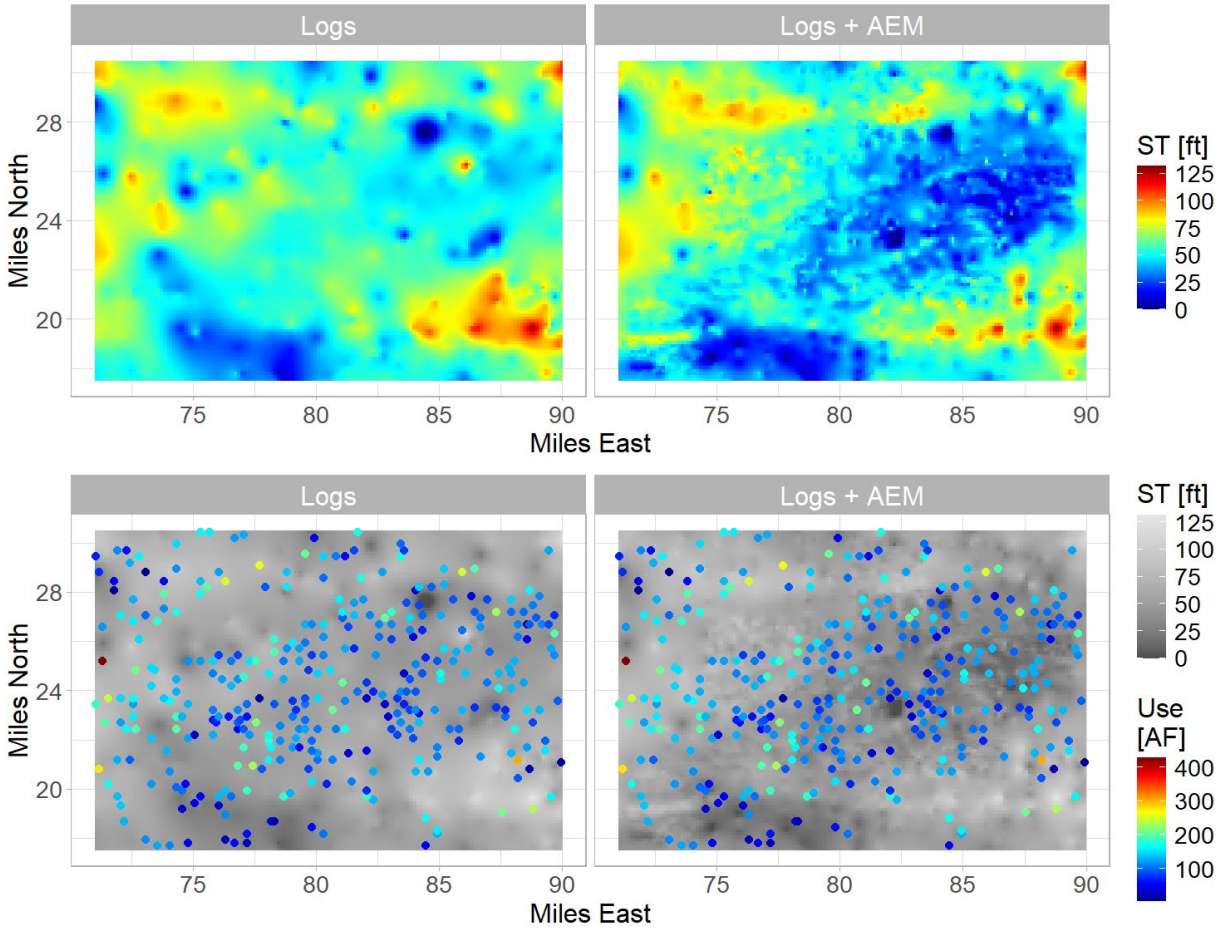


Figure 26. Average January 2020–2025 saturated thickness (ST, ft) computed from logs-only and combined dataset bedrock surfaces (top) and with 2020–2024 average irrigation water use (Use, acre-ft) superimposed (bottom) for Sheridan-6 focus area.

Comparison to Original Bedrock Surface

The original GMD4 flow model bedrock surface was developed by digitizing the contours from a 1995 USGS bedrock map and modifying those contours as needed to honor the available log-based bedrock picks (Macfarlane and Wilson, 2006). (These are the TS20-vintage bedrock picks in the data provided with this report.) The USGS map contours were not used in the development of the two bedrock surfaces presented in fig. 13 due to the inaccessibility of the primary source data used in the development of this map. To compare the new surfaces to the original, the bedrock elevations for the 16 fine grid cells in each model grid cell were averaged and compared to the original bedrock elevation for that model grid cell. Figure 27 shows the differences between each of the two new surfaces (after averaging to model grid cells) and the original surface, and fig. 28 depicts the distributions of these differences, with summary statistics given

in table 3. Overall, the spatial distributions of the differences are quite similar, although, not surprisingly, the combined-data differences in the vicinity of the AEM flight lines exhibit more variation. On average, the new logs-only bedrock surface is 1 foot above the original surface, and the combined-data surface is 2.5 feet above the original.

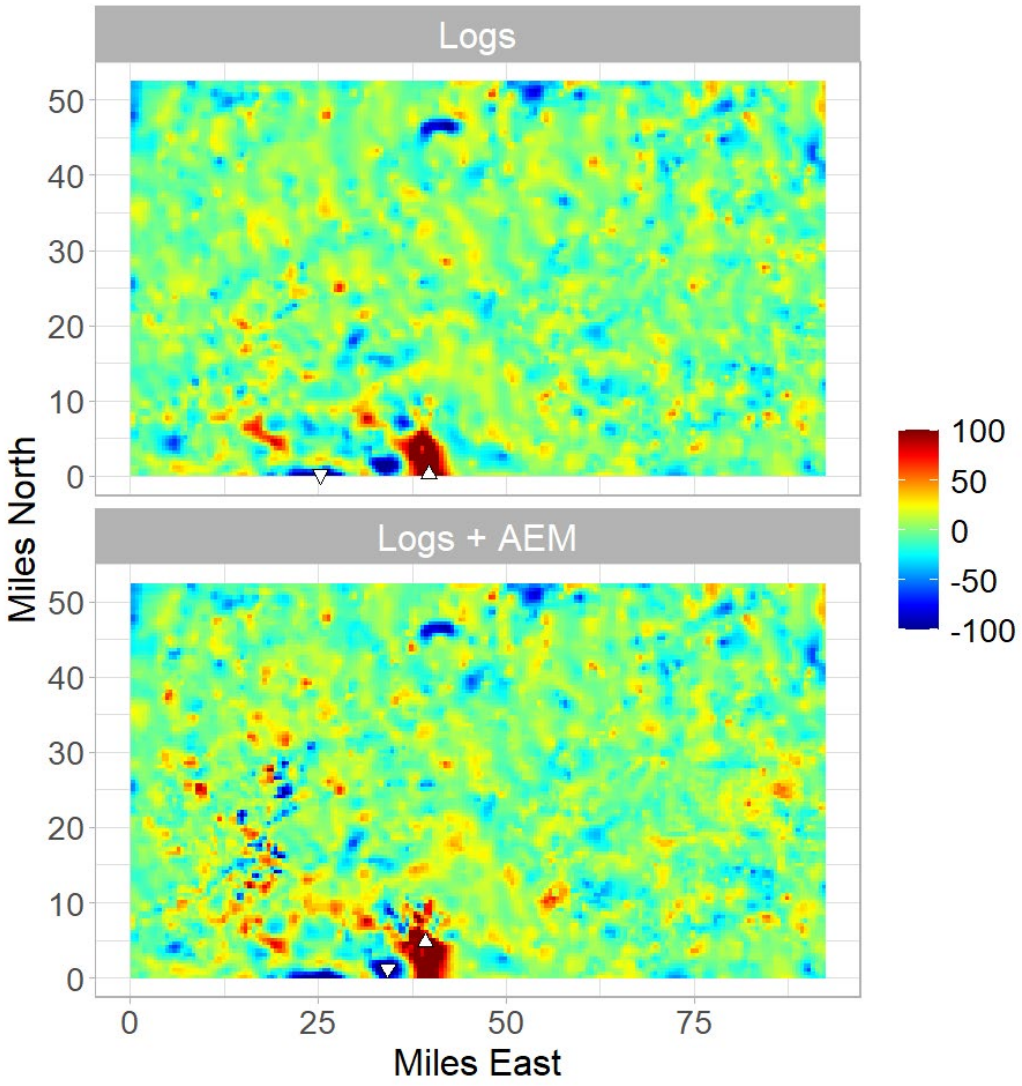


Figure 27. Difference (ft) between new bedrock surface and original bedrock surface based on logs alone and on combined dataset. Positive difference means new surface is above original and vice versa. The small percentage of cells with differences greater than 100 ft in magnitude (0.44% for logs-only, 0.56% for combined) are represented as -100 or 100 ft. Actual differences range from -119 to 210 ft for logs-only dataset and from -132 to 234 ft for combined dataset; downward and upward directed triangles indicate the locations of the minimum and maximum differences, respectively, in each case.

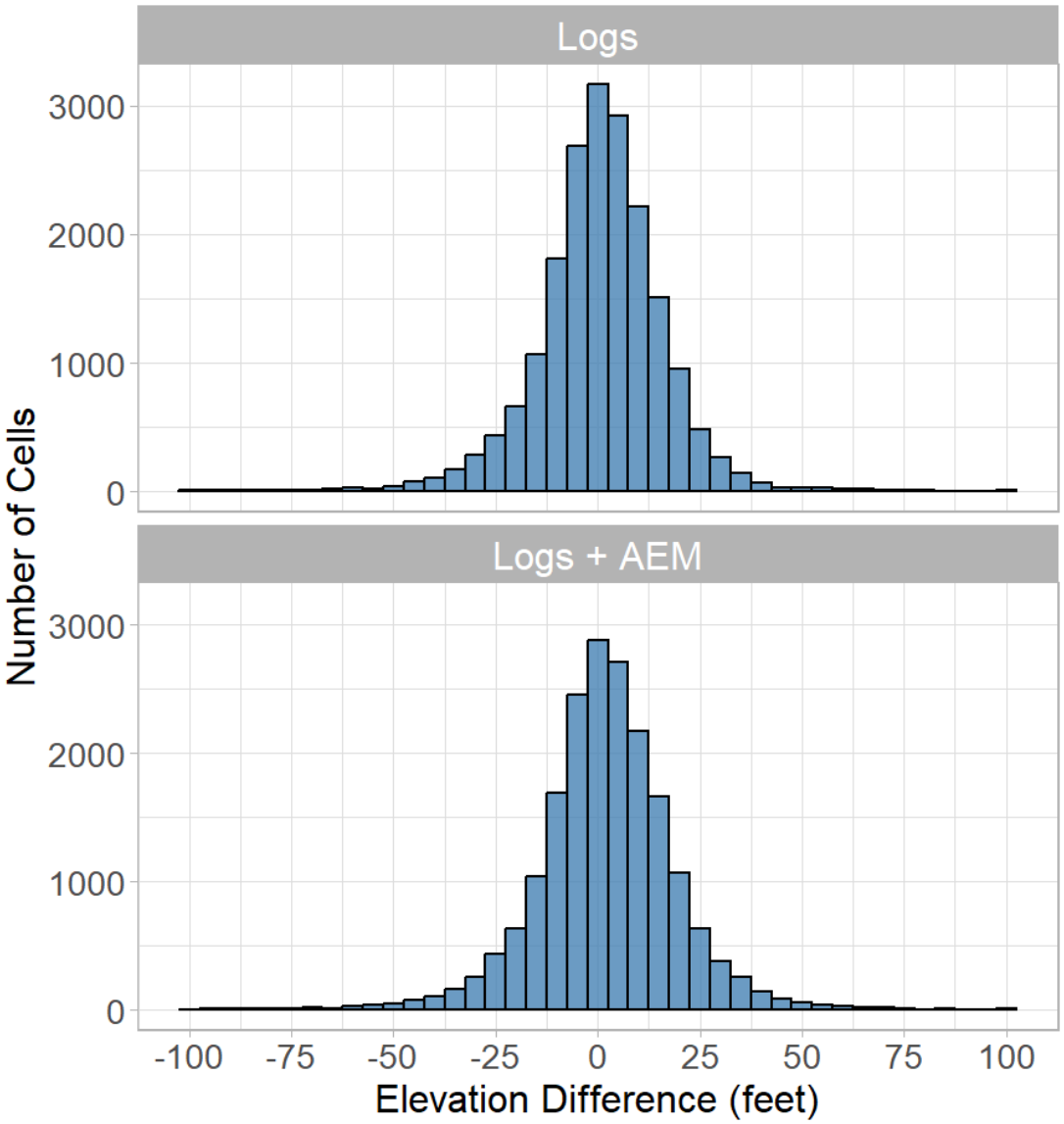


Figure 28. Histograms of differences shown in fig. 27. Bin width is 5 ft. The small percentage of cells with differences greater than 100 feet are excluded from the plot.

Table 3. Summary statistics (ft) of differences between bedrock surfaces developed in this report based on logs-only and combined (logs and AEM) datasets and original GMD4 flow model bedrock. Positive values indicate that the new surface is above the original and vice versa.

Data	Mean	SD	Min	5%	25%	50%	75%	95%	Max
Logs	1.0	18.4	-119.0	-25.5	-7.3	1.0	9.5	24.2	210.5
Logs + AEM	2.5	20.7	-131.7	-25.6	-7.0	2.1	11.7	30.2	233.9

Concentrated areas of large differences tend to occur near the edges of the study area where gaps exist in the log and/or AEM data, and the interpolation from these data involves a degree of extrapolation (compare fig. 27 to figs. 3 and 8). Due to gaps in the log data, the original bedrock surface in these areas would primarily reflect the USGS map contours, a data source not employed in the development of the new surfaces. It is interesting to note that the largest difference between the logs-only and original surfaces, 210 ft, occurs close to the southern edge of the grid in a data gap south of the Brownville focus area while the largest difference between the combined-data and original surface, 234 ft, is a few miles to the north in the Brownville focus area. This indicates that although the maximum discrepancy between the new log-based and original surfaces is probably impacted, at least to some degree, by extrapolation, the discrepancy is not out of keeping with the maximum difference between the combined-data and original surfaces, a difference that is supported by high-density AEM data. It seems likely that the original bedrock surface is in fact too low in this area (southern portion of the Brownville area and to the south of that).

Conclusions

Two lines of evidence indicate that integration of the AEM data provides a more accurate estimation of bedrock elevations than that provided by sediment logs alone: 1) The bedrock surface estimated using the combined log and AEM bedrock picks provides much clearer delineation of geologically plausible bedrock features. Specifically, this includes channel-like features in the southwest and Sheridan-6 focus areas and multiple small-scale depressions, possibly due to dissolution of underlying evaporites, in the Brownville and Thomas County index well areas. 2) The more detailed definition of bedrock topography provided by the addition of the AEM data leads to clearer correspondence between saturated thickness and irrigation water use. The improved estimate of saturated thickness provides an enhanced understanding of the region’s remaining groundwater resources.

Appendix A. Documentation of Datasets

Coordinates and Grid Specifications

The primary coordinate system used in the provided data files is a custom Albers projection developed for the western Kansas GMD flow models, including the GMD4 model. The X (west to east) and Y (south to north) coordinates are in feet. The provided data files also include the corresponding NAD83 latitude and longitude and NAD83 UTM Zone 14N coordinates.

The original model grid used half-mile grid cells (2,640 ft on a side). The fine grid employed in this study uses 1/8-mile grid cells (660 ft on a side) and is embedded in the original model grid, so that there are 16 fine-grid cells (a 4x4 block) in each model grid cell. The fine grid has 740 cells in the X direction and 420 in the Y direction. In the data files, the X- and Y-direction cell indices are represented as ix (ranging from 1 to 740) and iy (ranging from 1 to 420). In addition, the data files include an index that uniquely identifies each cell, given by ic = ix + 740 * (iy - 1). In the files containing irregularly distributed data points, these indices represent the grid cell that each data point falls in.

Several plots in this report show locations in terms of miles east and miles north of the fine grid origin (southwest corner of the southwestern-most cell), which, in model grid coordinates, is at (X,Y) = (-371271.1413 ft, 792067.3170 ft). This corresponds to UTM coordinates of (UTM.X, UTM.Y) = (231161.2083 m, 4326151.9501 m).

Data Files

The data files are available on this page:

https://www.kgs.ku.edu/Publications/OFR/2026/KGSOFR2026-38/index.html

Each dataset is provided as a csv file and as a layer in the ArcGIS map package GMD4Bedrock.mpkx, which is included on the page. The ArcGIS layers have the same names and contain the same columns (attributes) as the corresponding csv files.

The files are:

GMD4BedrockDataPoints.csv: Individual bedrock data points from sediment logs and AEM soundings. Columns are:

LogID: The log or AEM sounding ID. See discussion below.

County: County the log or AEM sounding is in. Kit Carson and Yuma counties are in Colorado and the rest are in Kansas.

Type: Log/sounding type—GeoLog for geological logs, WellLog for well logs, AEM for AEM soundings.

Vintage: Bedrock pick vintage—TS20 for log-based picks from Macfarlane and Wilson (2006), OFR26-38 for log-based picks made for this report, AEM for AEM-based picks.

Source: Data source: BULL for county geological bulletin, KBDR for Keene et al. (1969), WWC5 for WWC5 database, WIZD for WIZARD database, NWIS for USGS National Water Information System (Colorado logs), AEM for AEM.

Latitude, Longitude: NAD83 latitude, longitude.

UTM.X, UTM.Y: NAD83 Zone 14N coordinates (m).

X.ft, Y.ft: GMD4 model grid coordinates (ft).

ix, iy: X- and Y-direction indices of cell that point falls in.

ic: Unique index of cell that point falls in.

SurfElev.ft: Land surface elevation at the log/sounding location extracted from a LiDAR surface elevation raster (DASC, 2026).

BRDepth.ft: Bedrock depth pick in log or AEM sounding (ft).

BRElev.ft: Bedrock elevation (*SurfElev.ft* - *BRDepth.ft*) (ft).

For log-based bedrock picks made for this report (Vintage = OFR26-38), geological log IDs are in the township-range-section-quarters form used in several KGS county geological bulletins and Keene et al. (1969). For example, 6-38-26bca would represent a log in section 26 of township 6 south and range 38 west. All townships are south and all ranges are west, so direction designations are not required in the IDs. The letters represent successive quarter divisions, listed from largest to smallest area, with a = NE, b = NW, c = SW, and d = SE. In this case, the number of quarter subdivisions in the PLSS location (and thus the precision of the location information) is apparent from the ID. The log IDs for WWC5 logs of OFR26-38 vintage are the well IDs used in the WWC5 database. The information for a particular well can be obtained by substituting its well ID for nnnn at the end of this link:

https://chasm.kgs.ku.edu/ords/wwc5.wwc5d2.well_details?well_id=nnnn

Alternatively, the location and other information for all wells can be obtained by downloading wwc5_wells.zip (or wwc5_wells_full.zip) from the WWC5 web page:

https://www.kgs.ku.edu/Magellan/WaterWell/index.html

and extracting information for the wells of interest by linking to the table contained in that zip file through the well ID. Note that the quarter subdivisions in this table, in the column named

SPOT, are listed from smallest to largest rather than largest to smallest as in the geological log IDs. The corresponding logs are contained in wwc5_lith_log.zip on the same page.

CellAvgLogBRElevs.csv, CellAvgAEMBRElevs.csv, CellAvgComboBRElevs.csv: Bedrock elevations averaged over grid cells using logs alone, AEM alone, and logs and AEM combined, respectively. The columns in all three files are:

ix, iy: X- and Y-direction cell indices.
ic: Cell index (ix + 740 * (iy - 1)).
Count: Number of logs and/or AEM soundings in cell.
Latitude, Longitude: NAD83 latitude and longitude of average location of logs and/or AEM soundings in cell.
UTM.X, UTM.Y: NAD83 Zone 14N coordinates (m) of average location of logs and/or AEM soundings in cell.
X.ft, Y.ft: Model grid coordinates (ft) of average location of logs and/or AEM soundings in cell.
BRElev.ft: Bedrock elevation (ft above sea level) averaged over all logs and/or AEM soundings in cell.
BRRange.ft: Range of bedrock elevations (maximum - minimum) (ft) in cell.

Note that the locations represent the average of all locations in each grid cell, not the grid cell centers. If desired, the corresponding grid cell center locations could be computed as:

X.ft = -371271.1413 + 660 * (ix - 0.5)
Y.ft = 792067.3170 + 660 * (iy - 0.5)

or extracted by linking to the grid data (*FineGrid.csv*) through the cell index (*ic*).

FineGrid.csv: The gridded (interpolated) results. The columns are:

ix, iy: X- and Y-direction cell indices.
ic: Cell index (ix + 740 * (iy - 1)).
X.ft, Y.ft: Model grid coordinates (feet) of grid cell center.
Latitude, Longitude: NAD83 latitude and longitude of grid cell center.
UTM.X, UTM.Y: NAD83 Zone 14N coordinates (meters) of grid cell center.
SurfElev.ft: Land surface elevation (feet above sea level) for each fine grid cell bilinearly interpolated from model grid land surface elevations; model grid land surface elevations are averages of LiDAR land surface elevations over each grid cell.
WL.ft: Water level (feet above sea level) in grid cell interpolated from average of winter 2020–2025 water level measurements (*WaterLevels.csv*) to grid cells (see appendix B).

BRElevLogsKrg.ft: Bedrock elevations (ft above sea level) interpolated from cell-averaged log data (*CellAvgLogBRElevs.csv*) to grid cells (see Appendix B).
BRElevBothKrg.ft: Bedrock elevations (ft above sea level) interpolated from cell-averaged log + AEM data (*CellAvgComboBRElevs.csv*) to grid cells (see Appendix B).
SatThkLogs.ft: Saturated thickness (ft) computed log-based bedrock elevations (*WL.ft* - *BRElevLogsKrg.ft*, set to 0 where *WL.ft* < *BRElevLogsKrg.ft*).
SatThkBoth.ft: Saturated thickness (ft) computed log+AEM bedrock elevations (*WL.ft* - *BRElevBothKrg.ft*, set to 0 where *WL.ft* < *BRElevBothKrg.ft*).

WaterLevels.csv: Annual winter (mostly January) water level measurements from 2020 to 2025 and water level averaged across those years. Columns are:

Latitude, Longitude: NAD83 latitude and longitude of well.
UTM.X, UTM.Y: NAD83 Zone 14N coordinates (m) of well.
X.ft, Y.ft: Location of well in model grid coordinates (ft).
WL2020–WL2025: Annual water level measurements (ft above sea level) from 2020 to 2025.
WLAvg: Average of (non-missing) 2020–2025 water level measurements at well (ft above sea level).

IrrigationUse.csv: Annual irrigation water use (acre-ft) from 2020 to 2024 totaled over grid cells and average of those values over that period, for the 2,873 grid cells with active irrigation wells in that period. Columns are:

ix, iy: X- and Y-direction cell indices.
ic: Cell index (ix + 740 * (iy - 1)).
Count: Number of irrigation wells (technically, points of diversion) in grid cell with non-zero use for one or more years between 2020 and 2024.
Latitude, Longitude: NAD83 latitude and longitude of grid cell center.
UTM.X, UTM.Y: NAD83 Zone 14N coordinates (m) of grid cell center.
X.ft, Y.ft: Model grid coordinates (ft) of grid cell center.
IrrUse2020–IrrUse2024: Total annual irrigation water use (acre-ft) in grid cell from 2020 through 2024.
IrrUseAvg: Average use (acre-ft) in cell from 2020 to 2024 (average of *IrrUse2020–IrrUse2024*).

SWBox.csv, BVBox.csv, IWBox.csv, SDBox.csv: Coordinates of corner points of bounding boxes for southwest (SW), Brownville (BV), Thomas County index well (IW), and Sheridan-6

LEMA (SD) focus areas. The southwest corner of each box occurs at the beginning and end of each list to form a closed polygon. Columns are:

X.ft, Y.ft: Model grid coordinates (ft) of corner points.

These four bounding boxes are included in the FocusAreas layer in the ArcGIS map, GMD4Bedrock.aprx.

Appendix B: Interpolation Details

The interpolation approach used in this study is kriging, a geostatistical algorithm that aims to provide the maximum likelihood estimate of the property of interest (bedrock elevation in this case) at each estimation location (e.g., grid node) based on observed property values at nearby data locations (Goovaerts, 1997). Specifically, we have used the *krige* function implemented in the gstat library (Pebesma, 2004) for R (R Core Team, 2026). Kriging is generally implemented using a limited search neighborhood around each estimation location, and the optimal interpolation weights for the data points in that neighborhood are estimated based on the autocorrelation characteristics of the property. These characteristics are quantified using a semivariogram, which represents the average squared difference between observed values of the property as a function of the separation distance (referred to as "lag") between data points. In most cases, the semivariogram will increase with increasing lag distance, reflecting the tendency for differences between data values to grow with increasing separation. A model is then fit to the empirical semivariogram (computed from the data), and the model is used in the computation of the interpolation weights. Semivariogram models are selected from a limited set of "licit" models designed to ensure the solvability of the kriging equations; linear combinations of these licit models are also allowed.

The following R code can be used to reproduce the empirical and model semivariograms for the logs-only bedrock elevation data:

```
> # load the gstat library:
> library(gstat)
> # load data from csv file into data frame:
> CellAvgLogBR <- read.csv("CellAvgLogBRElevs.csv")
> # compute empirical semivariogram:
> CellAvgLogBR.vg <- variogram(BRElev.ft~X.ft+Y.ft, ~X.ft+Y.ft, CellAvgLogBR,
width=660, cutoff=200000)
> # fit model to empirical semivariogram:
> CellAvgLogBR.vgMod <- fit.variogram(CellAvgLogBR.vg, vgm(1600,"Sph",300000,
add.to=vgm(700,"Exp",8000,Err=100)))
> # look at fitted model:
> CellAvgLogBR.vgMod
 model   psill   range
1  Err  15.80267   0.00
2  Exp 478.83118  3667.91
3  Sph 2053.49475 268268.18
> # plot empirical (points) and model (line) semivariogram:
> plot(CellAvgLogBR.vg,CellAvgLogBR.vgMod)
```

The blue lines in the above code represent input, with ">" representing the console prompt and "#" used to introduce comments. The black lines represent output. The empirical semivariogram is computed using gstat's *variogram* function. The first argument to that function, `BRElev.ft~X.ft+Y.ft`, uses R's formula language to specify that we want to compute the

semivariogram of the bedrock elevation (BRElev.ft) after factoring out a linear trend in the model coordinates (X.ft and Y.ft). (In the formula language, the "+" is a means of listing terms in a model; it does not represent addition.) The bedrock elevation is dominated by an east-west trend, and we want to filter that to obtain a more stationary variable (residuals from the trend), which is more suitable for geostatistical analysis. The second argument to *variogram*, ~X.ft+Y.ft, uses R's formula language to state that the data point coordinates are represented by the variables X.ft and Y.ft. The third argument names the data frame to use in the analysis. The *width* argument specifies the nominal lag spacing to use (660 ft, the same as the grid cell size) and the *cutoff* argument specifies the maximum nominal lag (200,000 ft, somewhat less than half the maximum distance between data points).

The *fit.variogram* function is used to fit a model to the empirical semivariogram started from an initial model estimated from visual examination of the empirical semivariogram. The final fitted model, shown in the listing, has three components: 1) an error term essentially representing point-scale uncertainty (or noise) in the bedrock elevation values, with a partial sill (variance) of 15.8 ft^2, 2) an exponential component representing shorter-scale variation, with a partial sill of 478.8 ft^2 and a correlation length of 3,668 ft, and 3) a spherical component representing larger scale variation, with a partial sill of 2053.5 ft^2 and a range of 268,268 ft. Note that the value listed in the "range" column for the exponential component is in fact the correlation length, not the range; the practical range for this component is three times the correlation length, or 11,004 ft. Representing the point-scale variation as an error term rather than a more conventional nugget results in smooth rather than exact kriging, but this error term is so small that it makes little practical difference. The final line of code produces a rudimentary plot of the empirical and model semivariograms. A nicer plot is shown in fig. B1.

The following code repeats the semivariogram analysis for the combined (Logs + AEM) data:

```
> CellAvgComboBR <- read.csv("CellAvgComboBRElevs.csv")
> CellAvgComboBR.vg <- variogram(BRElev.ft~X.ft+Y.ft, ~X.ft+Y.ft, CellAvgComb
oBR, width=660, cutoff=200000)
> CellAvgComboBR.vgMod <- fit.variogram(CellAvgComboBR.vg, vgm(1600,"Sph",300
000,add.to=vgm(700,"Exp",8000)))
> CellAvgComboBR.vgMod
 model   psill   range
1  Exp 376.4646  2872.263
2  Sph 2635.3848 151543.532
> plot(CellAvgComboBR.vg,CellAvgComboBR.vgMod)
```

In this case a first-round fit including an error term resulted in an estimated error term of 0, so we have fit the model without including that term in the code above.

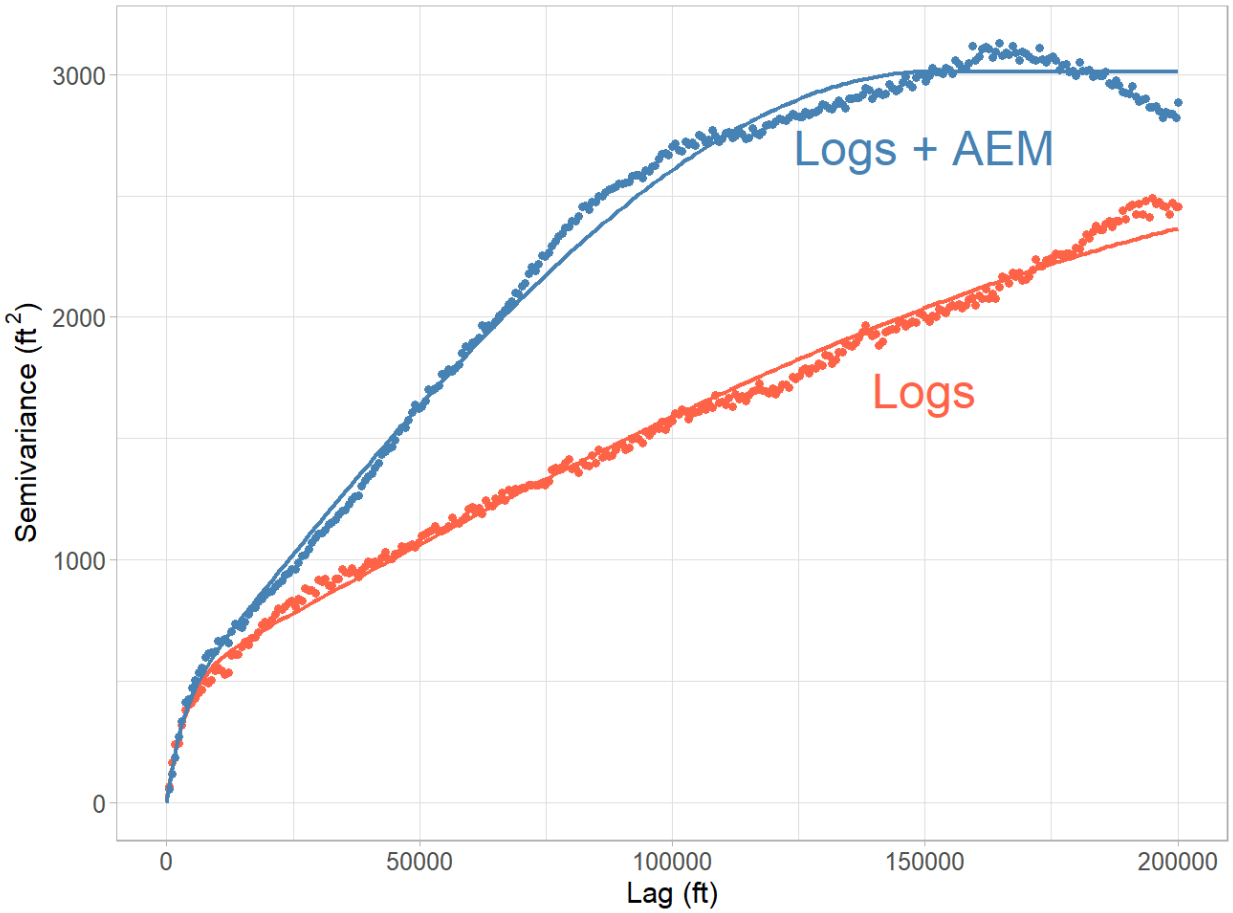


Figure B1. Semivariograms of linearly detrended cell-averaged bedrock elevations based on logs-only and combined datasets.

Figure B1 shows the logs-only and combined data semivariograms, which indicate that the combined-data bedrock elevations exhibit a higher overall level of variability (higher total sill) and have a shorter range than the logs-only data (logs-only semivariogram does not reach overall sill within the plot extent). That is, the combined-data bedrock elevations exhibit significantly more variation over shorter scales than the logs-only elevations.

Kriging of the logs-only and combined-data elevations to the fine grid can be accomplished using the following code (which takes some time to run); the FineGrid data file already contains both of these surfaces (shown in fig. 13 and documented in Appendix A), so the code below adds "V2" to the column names to avoid overwriting the original columns:

```
> # load the fine grid data:
> FineGrid <- read.csv("FineGrid.csv")
>
> # krige logs-only data to FineGrid, using "V2" to avoid overwriting
> # existing BRElevLogsKrg.ft:
> FineGrid$BRElevLogsKrgV2.ft <- krige(BRElev.ft~X.ft+Y.ft,
```

```
        ~X.ft+Y.ft, CellAvgLogBR, newdata=FineGrid,
        model=CellAvgLogBR.vgMod, omax=8,
        maxdist=1e12)$var1.pred
[using universal kriging]
> # set bedrock elevations above land surface to land surface:
> FineGrid$BRElevLogsKrgV2.ft <- pmin(FineGrid$BRElevLogsKrgV2.ft,
        FineGrid$SurfElev.ft)
>
> # krige combined-data elevations to FineGrid, using "V2" to avoid
> # overwriting BRElevBothKrg.ft:
> FineGrid$BRElevBothKrgV2.ft <- krige(BRElev.ft~X.ft+Y.ft,
        ~X.ft+Y.ft, CellAvgComboBR, newdata=FineGrid,
        model=CellAvgComboBR.vgMod, omax=8,
        maxdist=1e12)$var1.pred
[using universal kriging]
> # set bedrock elevations above land surface to land surface:
> FineGrid$BRElevBothKrgV2.ft <- pmin(FineGrid$BRElevBothKrgV2.ft,
        FineGrid$SurfElev.ft)
```

The first three arguments to the *krige* function are essentially the same as those for the *variogram* function, with the first argument stating that we want to krige accounting for a linear trend in X.ft and Y.ft and the third naming the data frame containing the points from which we are interpolating. The *newdata* argument is used to say that we are interpolating to the FineGrid data frame (which contains grid node coordinates named X.ft and Y.ft, matching the names in the original data). The *model* argument specifies the appropriate semivariogram model. The final two arguments specify the search neighborhood, with *omax* = 8 stating that we want to interpolate from a maximum of eight nearest neighboring points in each quadrant around the estimation location (the "o" actually represents "octant," but the octant search used in 3D interpolation reduces to a quadrant search in a 2D interpolation such as we are performing here) and *maxdist* = 1e12 specifying the maximum search radius (using a very large number, 1×10^{12}, to essentially eliminate the search radius restriction). Comparison of the "V2" kriged values to the original kriged values, BRElevLogsKrg.ft and BRElevBothKrg.ft, will verify reproduction of the original values (fig. 13).

The following code computes the empirical semivariogram for the 2020–2024 averaged annual water level measurements, fits a model to it, and then kriges water levels to the grid using that model:

```
> # read water levels into data frame named WL
> WL <- read.csv("WaterLevels.csv")
> # compute empirical semivariogram of 2020-2025 average WL:
> WLAvg.vg <- variogram(WLAvg~X.ft+Y.ft,~X.ft+Y.ft,WL,width=10000,cutoff=2500
00)
> # take alook at it:
> plot(WLAvg.vg)
> # fit model; R chooses best fit of three model forms
> # (exponential, spherical, Gaussian) listed
```

```
> WLAvg.vgMod <- fit.variogram(WLAvg.vg,vgm(2500,c("Exp","Sph","Gau"),10000))
> # look at resulting model (which is spherical):
> WLAvg.vgMod
 model  psill  range
1  Sph 2505.984 233973.1
> # krige to FineGrid (using all data, rather than limited neighborhood,
> # to get a nice smooth result);
> # using "v2" to avoid overwriting original WL.ft:
> FineGrid$WLv2.ft <- krige(WLAvg~X.ft+Y.ft,~X.ft+Y.ft,WL,newdata=FineGrid,mo
del=WLAvg.vgMod)$var1.pred
[using universal kriging]
> # limit to land surface elevation:
> FineGrid$WLv2.ft <- pmin(FineGrid$WLv2.ft,FineGrid$SurfElev.ft)
```

Again, comparison of WLv2.ft to the original interpolated surface, WL.ft, will verify reproduction of that surface.

References

Abraham, J.D., and Asch, T.H., 2024, Final spatially-constrained inversions report and data delivery from the 2024 airborne electromagnetic survey of a portion of Northwest Kansas Groundwater Management District #4, Aqua Geo Frameworks, LLC.

Bayne, C.K., 1956, Geology and ground-water resources of Sheridan County, Kansas: Kansas Geological Survey, Bulletin 116, 94 p. https://doi.org/10.17161/kgsbulletin.no.116.22103

DASC (Kansas Data Access and Support Center), 2026, Kansas elevation bare earth. https://hub.kansasgis.org/datasets/f3f6e09b96a54bbaab294ace74b35e74/explore?location=38.498077%2C-98.322312%2C7

Frye, J.C., 1945, Geology and ground-water resources of Thomas County, Kansas: Kansas Geological Survey, Bulletin 59, 111 p. https://doi.org/10.17161/kgsbulletin.no.59.21955

Goovaerts, P., 1997, Geostatistics for natural resources evaluation, Oxford University Press, 483 p.

Hodson, W.G., 1969, Geology and ground-water resources of Decatur County, Kansas: Kansas Geological Survey, Bulletin 196, 41 p. https://doi.org/10.17161/kgsbulletin.no.196.22221

Kang, S., and Knight, R., 2024, Imaging sediment-type variation in the High Plains aquifer system using airborne electromagnetic data. *Informal report*.

Keene, K.M, Pearl, R.H., and Pabst, M.E., 1969, Kansas ground water basic data release No. 1: hydrogeologic data from Cheyenne, Decatur, Rawlins, Sheridan, Sherman, and Thomas counties, Kansas: Kansas Geological Survey and U.S. Geological Survey.

Macfarlane, P.A. and Wilson, B.B., 2006, Enhancement of the bedrock-surface-elevation map beneath the Ogallala portion of the High Plains aquifer, western Kansas: Kansas Geological Survey, Technical Series 20, 36 p, 2 plates.

Miller, R.D., Buchanan, R., and Brosius, L., 1999, Measuring water levels in Kansas: Kansas Geological Survey, Public Information Circular 12, 4 p. https://kgs.ku.edu/measuring-water-levels-kansas

Pebesma, E.J., 2004, Multivariable geostatistics in S: The gstat package: Computers & Geosciences, v. 30, issue 7, p. 683–691. https://doi.org/10.1016/j.cageo.2004.03.012

Prescott, G.C., Jr., 1952, Geology and ground-water resources of Cheyenne County, Kansas: Kansas Geological Survey, Bulletin 100, 106 p. https://doi.org/10.17161/kgsbulletin.no.100.22060

Prescott, G.C., Jr., 1953, Geology and ground-water resources of Sherman County, Kansas: Kansas Geological Survey, Bulletin 105, 130 p. https://doi.org/10.17161/kgsbulletin.no.105.22078

R Core Team, 2026, R: A language and environment for statistical computing: R Foundation for Statistical Computing, Vienna, Austria. https://doi.org/10.32614/R.manuals

Suchy, D.R., 2002, The public land survey system in Kansas: Kansas Geological Survey, Public Information Circular 20, 4 p. https://kgs.ku.edu/public-land-survey-system-kansas

Walters, K.L., 1956, Geology and ground-water resources of Rawlins County, Kansas: Kansas Geological Survey, Bulletin 117, 100 p. https://doi.org/10.17161/kgsbulletin.no.117.22106

Wilson, B.B., Liu, G., Bohling, G.C., Whittemore, D., and Butler, J.J., Jr., 2015, West central Kansas GMD1 model: Kansas Geological Survey, Open-File Report 2015-33, 137 p. https://www.kgs.ku.edu/Hydro/Publications/2015/OFR15_33/OFR2015-33.pdf

Wilson, B.B., Liu, G., Bohling, G.C., and Butler, J.J., Jr., 2020, GMD2 groundwater flow model: High Plains aquifer modeling and maintenance project: Kansas Geological Survey, Open-File Report 2020-1, 94 p. https://www.kgs.ku.edu/Publications/OFR/2020/OFR2020-1.pdf

Wilson, B.B., Liu, G., Bohling, G.C., and Butler, J.J., Jr., 2021, GMD4 groundwater flow model: High Plains aquifer modeling and maintenance project: Kansas Geological Survey, Open-File Report 2021-6, 106 p. https://www.kgs.ku.edu/Publications/OFR/2021/OFR2021-6.pdf

Wilson, B.B., Liu, G., Bohling, G.C. and Butler, J.J., Jr., 2024, Update of the GMD3 groundwater flow model: High Plains aquifer modeling maintenance project: Kansas Geological Survey, Open-File Report 2024-14, 123 p. https://www.kgs.ku.edu/Publications/OFR/2024/OFR2024-14.pdf